The Astrophysical Journal, 705:1646–1671, 2009 November 10 doi:10.1088/0004-637X/705/2/1646

DEBRIS DISKS IN THE UPPER SCORPIUS OB ASSOCIATION

John M. Carpenter[1], Eric E. Mamajek[2], Lynne A. Hillenbrand[1], and Michael R. Meyer[3]
[1] California Institute of Technology, Department of Astronomy, MC 105-24, Pasadena, CA 91125, USA
[2] University of Rochester, Department of Physics and Astronomy, Rochester, NY, 14627-0171, USA
[3] Institute for Astronomy, ETH, CH-8093 Zurich, Switzerland
Received 2009 July 12; accepted 2009 September 29; published 2009 October 26

ABSTRACT

We present MIPS 24 μm and 70 μm photometry for 205 members of the Upper Scorpius OB Association. These data are combined with published MIPS photometry for 15 additional association members to assess the frequency of circumstellar disks around 5 Myr old stars with spectral types between B0 and M5. Twelve stars have a detectable 70 μm excess, each of which also has a detectable 24 μm excess. A total of 54 stars are identified with a 24 μm excess more than 32% above the stellar photosphere. The MIPS observations reveal 19 excess sources—8 A/F/G stars and 11 K/M stars—that were not previously identified with an 8 μm or 16 μm excess. The lack of short-wavelength emission and the weak 24 μm excess suggests that these sources are debris systems or the remnants of optically thick primordial disks with inner holes. Despite the wide range of luminosities of the stars hosting apparent debris systems, the excess characteristics are consistent with all stars having dust at similar orbital radii after factoring in variations in the radiation blowout particle size with spectral type. The results for Upper Sco are compared to similar photometric surveys from the literature to re-evaluate the evolution of debris emission. After considering the completeness limits of published surveys and the effects of stellar evolution on the debris luminosity, we find that the magnitude of the 24 μm excess around F-type stars increases between ages of 5 and 17 Myr as found by previous studies, but at $\lesssim$2.6σ confidence. For B7-A9 and G0-K5 stars, any variations in the observed 24 μm excess emission over this age range are significant at less than 2σ confidence.

Key words: circumstellar matter – open clusters and associations: individual (Upper Scorpius) – planetary systems: formation – planetary systems: protoplanetary disks – stars: pre-main sequence

Online-only material: machine-readable tables

1. INTRODUCTION

Dusty debris observed around main-sequence stars is a potential diagnostic of planetary systems. The current paradigm is that the debris originates from the collisional grinding of planetesimals to micron-sized grains, where the collision rate is dictated by gravitational interactions between planets and a planetesimal belt (Williams & Wetherill 1994). If this hypothesis is correct, the spatial asymmetries in the debris that have been revealed by high-resolution imaging (e.g., Holland et al. 1998) encodes information on the eccentricity, mass, and even migration of the orbiting planets (Liou & Zook 1999; Wyatt 2003). Unfortunately, the resolution and sensitivity required to image the debris can be achieved for only a few disks with current instruments.

A complementary approach to detailed studies of individual disks is to study the ensemble properties of debris systems. Debris disks have been studied extensively over the entire sky using *IRAS* (Backman & Paresce 1993; Lagrange et al. 2000; Rhee et al. 2007) and in targeted regions using the *Infrared Space Observatory* (*ISO*; Habing et al. 2001; Spangler et al. 2001; Dominik & Decin 2003). The *Spitzer Space Telescope* (Werner et al. 2004) has expanded on these studies to produce a vast database of debris disks (e.g., Rieke et al. 2005; Bryden et al. 2006; Su et al. 2006; Gautier et al. 2007; Currie et al. 2008a; Carpenter et al. 2009, see also reviews by Werner et al. 2006, Meyer et al. 2007 and Wyatt 2008) that encompass a broad range of spectral types (B-M stars), environments (clusters, associations, field stars), and ages (3 Myr to 10 Gyr). Comparison of these data to theoretical models have yielded insights on the planetesimal belts that produce the debris dust (Wyatt et al. 2007b), the collisional history of planetesimal belts (Dominik & Decin 2003; Wyatt et al. 2007a; Löhne et al. 2008) and the formation of planetary systems (Kenyon & Bromley 2008, and references therein).

A critical issue emerging from *Spitzer* studies is establishing when the debris phenomenon is initiated. In the Kenyon & Bromley models, a planetesimal belt produces low levels of debris emission in the early stage of planetary accretion. At a given orbital radius, dust production reaches a maximum when 1000–3000 km sized bodies form and ignite the destructive collisional cascade (Kenyon & Bromley 2004). As planet formation propagates through the disk, the disk is depleted of planetesimals through repeated collisions and the debris production eventually declines. In theory, the evolution of the debris emission can constrain the formation time of planets and the collisional cascade. Indeed, based on *Spitzer* observations, Hernández et al. (2006) and Currie et al. (2008a) have suggested that the debris luminosity peaks around 10–30 Myr for A-F stars before declining toward older ages (Rieke et al. 2005).

Additional observations are needed to validate previous conclusions since few surveys for debris emission at ages of $\lesssim$10 Myr have been completed (Hernández et al. 2006; Carpenter et al. 2006; Gautier et al. 2008; Currie et al. 2009). The Upper Scorpius OB Association (hereafter, Upper Sco) is an important region in studies of disk evolution since it provides a snapshot of disk properties at an age of ~5 Myr when most optically thick disks have dissipated (Hernández et al. 2007). *Spitzer* observations can then probe the onset of debris production as planets form. Since association members have been identified from B to M stars, disk properties can be investigated over nearly two orders of magnitude in stellar mass. Finally, at a mean distance of 145 pc (de Zeeuw et al. 1999), Upper Sco is more than a factor of 2 closer than other clusters or associations of similar age. These traits permit sensitive photometric studies of debris properties.

In previous studies, we investigated the 4.5–16 μm photometric (Carpenter et al. 2006, hereafter Paper I) and 5–35 μm spectroscopic (Dahm & Carpenter 2009) properties of circumstellar disks in Upper Sco. The principal result from these studies is that the circumstellar disks detected at wavelengths shortward of 16 μm show a dichotomy with spectral type. Circumstellar disks around late-type stars (K and M spectral types) are likely optically thick primordial disks formed as a result of the star formation process, while early-type stars (B and A types) appear to be surrounded by debris disks. Surprisingly, no disks were detected around the F and G stars.

The photometric data presented in Paper I spanned wavelengths between 4.5 μm and 16 μm. To probe for cooler dust, we present here 24 μm and 70 μm photometric observations of 205 Upper Sco members. These new *Spitzer* observations of Upper Sco are presented in Section 2. In Section 3, we use these data to identify stars that have excesses in the 24 μm and 70 μm bands. The nature of the excess sources is investigated in Section 4, and properties of debris systems around stars with a wide range in mass are compared in Section 5. In Section 6, we compare the Upper Sco results with published *Spitzer* surveys to investigate the evolution of debris systems.

2. OBSERVATIONS AND DATA REDUCTION

The selection criteria for the Upper Sco sample are described in Paper I. Briefly, the sample was constructed from membership lists established by Hipparcos astrometry (de Zeeuw et al. 1999), color–magnitude diagrams (Preibisch & Zinnecker 1999; Preibisch et al. 2002), and X-ray surveys (Walter et al. 1994; Martín 1998; Preibisch et al. 1998; Kunkel 1999; Köhler et al. 2000). Since membership selection was based upon stellar properties (proper motions, photospheric colors, X-ray activity) unrelated to circumstellar disks, the sample is believed to be unbiased with respect to the presence or absence of disks. From the compiled list, we selected 205 stars[4] to sample spectral types between B0 and M5. This sample was supplemented with 15 Upper Sco members with G/K spectral types that were observed by the Formation and Evolution of Planetary Systems (FEPSs) *Spitzer* Legacy program (Meyer et al. 2006). The FEPS targets were selected based on similar criteria as our study and should also be an unbiased sample with respect to the presence or absence of disks.

Other Upper Sco members have been observed with *Spitzer* but are not included in our sample. The Herbig Ae/Be star HIP 79476 (Hernández et al. 2005) was observed with the *Spitzer* Infrared Spectrograph (IRS), but not with the Multiband Imaging Photometer for *Spitzer* (MIPS). We did not include the G6/G8 star HD 143006, which was also observed by the FEPS program as part of survey of gas in disks. HD 143006 was recognized as a Upper Sco member based on an *IRAS* excess (Odenwald 1986) and thus would bias the sample. We also do not use the three B stars observed by Rieke et al. (2005) and the five F/G stars observed by Chen et al. (2005) since IRAC data are not available for these sources, which is needed for the analysis presented in Section 3. Finally, we did not include brown-dwarfs in Upper Sco (Scholz et al. 2007).

In Paper I, IRAC (4.5 μm and 8 μm) and IRS peak-up (16 μm) photometry was presented for 218 of the 220 stars. IRAC photometry for one additional Upper Sco member observed by FEPS (ScoPMS 52) is now available (Carpenter et al. 2008). The remaining star (HIP 80112) was not observed with IRAC since it would have saturated the detector. The 4.5 μm flux density for this source was estimated from ground-based *M*-band observations (van der Bliek et al. 1996).

We present here MIPS 24 μm and 70 μm photometry for 205 stars in Upper Sco. The data reduction procedures follow that used by the FEPS program as described in Carpenter et al. (2008), and a only summary of the salient steps is provided here. Table 1 presents the 24 μm and 70 μm MIPS photometry for the 205 stars observed for this study. MIPS photometry for the remaining 15 stars are listed in Carpenter et al. (2008).

2.1. MIPS 24 μm

MIPS 24 μm observations for 205 stars were obtained in photometry mode. The exposure time per image (either 3 or 10 s) and the number of dithered images were set to achieve a signal-to-noise ratio of at least 10 on the expected photospheric brightness. MIPS 24 μm images were processed starting with the Basic Calibrated Data (BCD) products produced by the *Spitzer* Science Center (SSC) pipeline version S17. Individual BCD images were combined to derive a flat field that removed long-term gain changes in the MIPS array. Flat field images were derived from stars that are not surrounded by nebulosity. If nebulosity is present, a flat-field image from another star was used that was observed close in time and with the same exposure time.

Point(source)-response-function (PRF) photometry was performed with the MOPEX package (Makovoz & Marleau 2005). The empirical PRF distributed with MOPEX was fitted to the individual BCD images simultaneously (as opposed to the mosaicked image) using a fitting area of 21×21 pixels (1 pixel ≈ 2.″55) for most sources. A 5×5 pixel fitting area was used for sources that have spatially variable nebulosity near the point source position. From visual inspection of the mosaicked images, the PRF of the Upper Sco target overlaps occasionally with that from a nearby source. These contaminating sources were fitted with a PRF simultaneously. The measured 24 μm flux densities and internal uncertainties from the PRF fit are presented in Table 1. The images were processed with a calibration factor of 0.0447 MJy sr^{-1}. Following Engelbracht et al. (2007), we adopt a calibration uncertainty of 4%.

Cirrus and extragalactic sources may contaminate the MIPS photometry and create the appearance of an infrared excess. Since we expect the emission from a circumstellar disk to be point-like and centered on the star at the distance of Upper Sco, contaminated 24 μm photometry can be identified from emission that is extended or offset from the stellar position.

The maximum astrometric offset between the Two Micron All Sky Survey (2MASS) and *Spitzer* 24 μm positions is 1.″6 for HIP 78820. The dispersion in the offsets is the same (∼0.4 to 0.″55) for stars with and without infrared excesses (see Section 3.1), indicating that any contamination is not systematically producing offsets in the measured coordinates. This empir-

[4] Bouy & Martín (2009) found that the star [PBB2002] USco 161021.5−194132 deviates from the mean proper motion for Upper Sco and may be an interloper. The reduced χ^2 from the 2MASS point-spread function fitting photometry is the second highest among the nearest 100 stars to this source that have a 2MASS quality flag of AAA. The astrometry may therefore be contaminated by a binary. The luminosity of this star is also higher than the 10 nearest stars of the same spectral type (Preibisch et al. 2002), consistent with a binary contaminant. Given that the lithium equivalent width (Preibisch et al. 2002) and apparent brightness are consistent with Upper Sco membership, we retain the source in our sample.

Table 1
MIPS 24 and 70 μm Photometery

Source[a]	MIPS 24 μm[b]		MIPS 70 μm[c]		AORKEY	Flags
	S_ν (mJy)	σ (mJy)	S_ν (mJy)	σ (mJy)		
HD 142987	7.89	0.07	5.2	11.5	13908224	
HD 147810	9.67	0.09	−8.7	10.2	13906432	
HD 149598	5.56	0.05	11.0	21.6	13909504	
HIP 76071	10.79	0.10	−11.4	8.8	13902848	
HIP 76310	165.40	1.50	373.1	11.3	13904896	
HIP 76633	9.26	0.08	12.0	9.0	13907968	
HIP 77457	8.63	0.08	14.7	12.2	13906688	
HIP 77545	9.48	0.09	59.3	58.5	13899264	
HIP 77635	79.15	0.71	−18.1	28.3	13899264	
HIP 77815	10.85	0.10	0.0	12.7	13901568	
HIP 77840	68.72	0.62	−58.5	25.9	13899264	1
HIP 77858	46.93	0.42	−5.1	23.5	13899776	3
HIP 77859	91.89	0.83	−18.4	15.2	13899776	
HIP 77900	19.55	0.18	−12.5	10.2	13901056	
HIP 77909	25.76	0.23	4.2	15.9	13899264	
HIP 77911	142.60	1.30	253.1	10.5	13901568	
HIP 77960	8.49	0.08	−15.6	9.5	13901568	
HIP 78099	12.98	0.12	−21.8	10.0	13901568	
HIP 78104	105.50	0.90	0.5	9.7	13898752	
HIP 78168	34.18	0.31	20.4	13.4	13900288	5
HIP 78196	10.05	0.09	−1.4	7.3	13903616	
HIP 78207	766.40	7.30	233.3	25.4	13899008	
HIP 78233	6.22	0.06	−2.0	8.8	13900288	
HIP 78246	35.33	0.32	15.6	11.9	13900032	
HIP 78265	277.90	3.10	5.2	88.2	13897472	1
HIP 78483	8.04	0.07	7.1	15.7	13897472	
HIP 78494	11.74	0.11	−13.8	11.7	13900032	
HIP 78530	13.10	0.12	2.2	17.9	13902336	
HIP 78549	12.20	0.11	−9.6	12.9	13902336	
HIP 78702	11.90	0.11	2.4	9.6	13905408	
HIP 78809	8.54	0.08	−9.3	13.1	13900544	5
HIP 78820	451.70	4.10	46.5	13.4	13896960	
HIP 78847	10.42	0.09	5.7	10.7	13902336	
HIP 78877	31.33	0.28	−3.0	24.8	13900544	
HIP 78933	144.80	1.30	−4.0	19.4	13898240	
HIP 78956	14.92	0.13	1.0	10.8	13905152	
HIP 78963	8.85	0.08	14.7	14.8	13907200	
HIP 78968	14.72	0.13	−2.2	11.7	13905152	5
HIP 78996	35.87	0.32	9.4	10.7	13900544	
HIP 79083	17.87	0.16	−3.8	9.7	13898240	
HIP 79097	10.20	0.09	−6.0	9.9	13906176	
HIP 79124	12.64	0.11	0.7	15.3	13903104	
HIP 79156	22.62	0.20	5.5	9.4	13897984	
HIP 79250	12.02	0.11	−25.2	12.0	13905920	5
HIP 79366	9.27	0.08	2.6	13.2	13905920	
HIP 79374	212.20	1.90	12.0	21.3	13897984	
HIP 79392	7.28	0.07	2.4	12.5	13900800	
HIP 79404	64.91	0.58	−48.1	21.4	13899520	1
HIP 79410	41.25	0.37	8.1	11.9	13897984	
HIP 79439	23.86	0.21	32.8	15.4	13897984	
HIP 79462	15.11	0.14	−3.8	10.6	13905920	
HIP 79530	24.74	0.22	3.5	14.0	13900800	
HIP 79606	11.48	0.10	−12.0	14.3	13904128	
HIP 79643	9.30	0.08	0.5	10.2	13900800	
HIP 79644	3.03	0.04	−16.7	9.8	13901312	
HIP 79733	5.09	0.05	−2.0	9.9	13899520	
HIP 79739	11.47	0.10	−17.7	22.3	13900800	
HIP 79771	10.63	0.10	−22.5	37.0	13904640	
HIP 79785	18.61	0.17	−6.7	13.7	13901312	
HIP 79860	5.26	0.05	−0.8	9.4	13908992	
HIP 79878	33.90	0.31	26.1	15.9	13903872	
HIP 79897	12.40	0.11	1.7	10.6	13903360	5
HIP 80024	48.03	0.43	−13.3	100.3	13901824	
HIP 80059	8.00	0.07	−18.8	11.9	13901312	
HIP 80088	22.62	0.20	79.2	13.8	13903360	

Table 1
(Continued)

Source[a]	MIPS 24 μm[b]		MIPS 70 μm[c]		AORKEY	Flags
	S_ν (mJy)	σ (mJy)	S_ν (mJy)	σ (mJy)		
HIP 80112	717.90	7.80	209.4	507.6	13896704	
HIP 80130	9.04	0.08	2.3	12.3	13907456	
HIP 80311	4.25	0.04	4.6	23.1	13902080	
HIP 80324	11.37	0.10	6.6	13.8	13902592	
HIP 80338	24.91	0.25	168.2	42.9	13902080	3, 4
HIP 80493	11.50	0.10	5.2	22.6	13904384	
HIP 80896	8.09	0.07	26.4	10.2	13907712	
HIP 81266	267.20	2.40	−8.8	49.6	13897728	
HIP 82319	5.60	0.05	6.3	8.5	13908736	
HIP 82397	17.90	0.16	−4.5	11.9	13906944	
[PBB2002] USco J155624.8−222555	23.98	0.22	12.8	9.5	13914368	
[PBB2002] USco J155625.7−224027	0.84	0.03	2.1	12.6	13912832	
[PBB2002] USco J155629.5−225657	0.82	0.03	4.5	10.8	13912832	
[PBB2002] USco J155655.5−225839	1.89	0.04	2.8	9.8	13901568	
[PBB2002] USco J155706.4−220606	7.60	0.07	14.5	9.8	13916672	
[PBB2002] USco J155729.9−225843	6.10	0.06	25.3	12.5	13916416	
[PBB2002] USco J155746.6−222919	0.91	0.03	−0.6	14.9	13912832	
[PBB2002] USco J155829.8−231007	24.53	0.22	6.9	10.9	13916928	
[PBB2002] USco J155918.4−221042	1.17	0.04	1.5	9.2	13902336	
[PBB2002] USco J160159.7−195219	0.33	0.01	8.1	8.3	15728128	
[PBB2002] USco J160210.9−200749	0.29	0.01	−6.9	9.3	13917952	
[PBB2002] USco J160222.4−195653	0.69	0.02	7.3	9.7	15729664	
[PBB2002] USco J160226.2−200241	0.49	0.02	1.1	8.8	15729152	
[PBB2002] USco J160245.4−193037	0.45	0.02	−0.1	10.3	13915904	5
[PBB2002] USco J160329.4−195503	0.54	0.02	−0.1	12.3	15729152	5
[PBB2002] USco J160341.8−200557	1.76	0.04	−3.1	9.7	13905408	
[PBB2002] USco J160343.3−201531	1.40	0.04	5.9	12.1	13905408	
[PBB2002] USco J160350.4−194121	0.68	0.03	−2.5	7.9	15727872	
[PBB2002] USco J160357.9−194210	25.65	0.23	26.9	10.3	13912064	
[PBB2002] USco J160418.2−191055	0.58	0.03	−15.9	12.3	15729664	
[PBB2002] USco J160428.4−190441	2.31	0.04	−3.2	9.1	15729920	
[PBB2002] USco J160435.6−194830	0.51	0.02	0.6	8.6	15728896	
[PBB2002] USco J160439.1−194245	0.87	0.02	−2.1	9.0	15727616	
[PBB2002] USco J160449.9−203835	0.59	0.02	−5.2	9.0	15727360	
[PBB2002] USco J160456.4−194045	0.64	0.03	9.8	9.2	15729664	
[PBB2002] USco J160502.1−203507	1.95	0.04	4.2	11.2	13898240	
[PBB2002] USco J160508.3−201531	1.79	0.04	−14.1	10.8	13905408	
[PBB2002] USco J160516.1−193830	0.30	0.01	−2.1	10.5	13917952	
[PBB2002] USco J160517.9−202420	2.42	0.04	4.1	9.8	13898240	
[PBB2002] USco J160521.9−193602	0.98	0.04	6.0	9.2	13905408	
[PBB2002] USco J160525.5−203539	5.95	0.05	1.1	11.0	15727104	
[PBB2002] USco J160528.5−201037	1.07	0.04	−4.1	9.9	13905408	
[PBB2002] USco J160531.3−192623	0.35	0.01	4.6	8.9	15728128	
[PBB2002] USco J160532.1−193315	3.92	0.04	19.3	9.9	15726848	
[PBB2002] USco J160545.4−202308	26.22	0.24	31.9	11.7	13912064	
[PBB2002] USco J160600.6−195711	14.28	0.13	17.3	8.5	13912064	
[PBB2002] USco J160611.9−193532	0.50	0.02	2.8	9.7	15729152	
[PBB2002] USco J160619.3−192332	0.29	0.01	−15.5	9.6	15728384	
[PBB2002] USco J160622.8−201124	19.63	0.18	16.3	11.9	15729152	
[PBB2002] USco J160628.7−200357	0.89	0.03	14.6	9.9	13912064	
[PBB2002] USco J160643.8−190805	12.89	0.12	12.2	8.7	15729920	
[PBB2002] USco J160647.5−202232	1.30	0.04	−7.6	9.7	13898240	
[PBB2002] USco J160702.1−201938	8.65	0.08	7.2	11.9	15728640	
[PBB2002] USco J160704.7−201555	0.32	0.01	−2.0	10.1	15728640	
[PBB2002] USco J160707.7−192715	1.60	0.04	−5.2	9.1	15729920	
[PBB2002] USco J160708.7−192733	0.56	0.02	5.0	8.4	15728896	
[PBB2002] USco J160719.7−202055	0.84	0.02	0.1	10.4	15729408	
[PBB2002] USco J160739.4−191747	3.27	0.04	7.7	10.3	13903104	
[PBB2002] USco J160801.4−202741	2.23	0.04	0.6	13.7	13898240	
[PBB2002] USco J160801.5−192757	1.58	0.04	−4.1	9.6	15729920	
[PBB2002] USco J160802.4−202233	0.77	0.03	1.7	10.6	13913088	
[PBB2002] USco J160804.3−194712	0.47	0.03	−10.2	11.1	13913088	
[PBB2002] USco J160815.3−203811	0.73	0.03	−16.1	10.8	15729408	
[PBB2002] USco J160818.4−190059	1.05	0.04	8.3	10.0	13903104	

Table 1
(Continued)

Source[a]	MIPS 24 μm[b]		MIPS 70 μm[c]		AORKEY	Flags
	S_ν (mJy)	σ (mJy)	S_ν (mJy)	σ (mJy)		
[PBB2002] USco J160823.2−193001	76.90	0.69	99.9	10.7	13903104	
[PBB2002] USco J160823.5−191131	1.34	0.04	7.2	11.9	13903104	
[PBB2002] USco J160823.8−193551	2.26	0.04	8.9	8.6	15729920	
[PBB2002] USco J160825.1−201224	1.27	0.04	3.3	11.5	13911040	
[PBB2002] USco J160827.5−194904	8.91	0.08	15.8	9.7	13913088	
[PBB2002] USco J160843.1−190051	0.99	0.04	−15.5	10.2	13903104	
[PBB2002] USco J160854.0−203417	1.26	0.04	9.7	14.3	13898240	
[PBB2002] USco J160900.0−190836	21.17	0.19	6.1	11.8	13914880	5, 6
[PBB2002] USco J160900.7−190852	285.80	2.60	251.3	12.5	13903104	
[PBB2002] USco J160903.9−193944	0.76	0.03	2.0	8.6	13912320	
[PBB2002] USco J160904.0−193359	0.62	0.02	0.9	9.9	13914880	
[PBB2002] USco J160913.4−194328	0.66	0.03	−6.6	9.9	13913088	
[PBB2002] USco J160915.8−193706	0.33	0.01	6.6	10.6	15728384	
[PBB2002] USco J160933.8−190456	1.44	0.04	−22.0	13.7	13903104	
[PBB2002] USco J160946.4−193735	1.55	0.04	2.3	12.8	13897984	
[PBB2002] USco J160953.6−175446	9.17	0.08	14.8	10.8	15726592	
[PBB2002] USco J160954.4−190654	2.35	0.04	22.3	15.2	13897984	
[PBB2002] USco J160959.4−180009	113.60	1.00	127.6	15.2	13912576	
[PBB2002] USco J161010.4−194539	0.87	0.03	6.9	10.2	13912320	
[PBB2002] USco J161011.0−194603	0.78	0.01	2.4	12.5	13917440	
[PBB2002] USco J161014.7−191909	1.68	0.04	2.9	11.0	13897984	
[PBB2002] USco J161021.5−194132	1.52	0.04	−15.7	11.1	13897984	
[PBB2002] USco J161024.7−191407	0.80	0.03	7.4	12.5	13912320	
[PBB2002] USco J161026.4−193950	0.85	0.03	−3.5	10.2	13912320	
[PBB2002] USco J161031.9−191305	3.05	0.04	5.3	20.3	13897984	
[PBB2002] USco J161052.4−193734	1.14	0.03	9.6	11.3	13914112	1
[PBB2002] USco J161115.3−175721	72.82	0.66	18.1	11.8	13910784	
[PBB2002] USco J161118.1−175728	2.29	0.05	−15.1	11.7	13910784	
[PBB2002] USco J161420.2−190648	1170.00	11.00	630.1	24.8	13908480	5
PPM 732705	3.65	0.04	−6.8	11.4	13910016	
PPM 747651	3.63	0.04	14.1	8.7	13910272	
PPM 747978	2.90	0.06	0.9	15.7	13910528	
[PZ99] J153557.8−232405	1.39	0.04	0.8	10.0	13911808	
[PZ99] J154413.4−252258	2.39	0.05	−12.5	13.5	13905664	
[PZ99] J155106.6−240218	1.52	0.07	−16.9	11.9	13899776	
[PZ99] J155716.6−252918	2.82	0.04	−3.8	14.8	13897472	
[PZ99] J155750.0−230508	1.88	0.04	7.3	10.2	13901568	5
[PZ99] J155812.7−232835	14.42	0.13	31.1	42.5	13909248	
[PZ99] J1600.00.7−250941	2.71	0.04	13.9	16.0	13897472	
[PZ99] J160013.3−241810	2.45	0.04	−13.0	10.2	13900032	
[PZ99] J160031.3−202705	3.02	0.04	−1.9	9.9	13900288	
[PZ99] J160042.8−212737	2.60	0.04	1.8	10.4	13900288	
[PZ99] J160108.0−211318	3.25	0.04	−0.3	9.3	13900288	
[PZ99] J160147.4−204945	4.07	0.04	−3.4	11.6	13900288	
[PZ99] J160200.3−222123	4.56	0.04	−10.4	10.7	13902336	
[PZ99] J160239.1−254208	2.11	0.04	4.7	16.3	13897472	
[PZ99] J160251.2−240156	2.91	0.07	−12.8	14.7	13900544	
[PZ99] J160354.9−203137	3.69	0.17	−0.6	12.1	13909760	5
[PZ99] J160357.6−203105	328.00	3.00	187.8	12.7	13909760	
[PZ99] J160421.7−213028	167.50	1.50	1917.4	24.8	13902336	
[PZ99] J160539.1−215230	1.87	0.04	−2.1	12.4	13902336	
[PZ99] J160612.5−203647	2.88	0.04	0.5	10.9	13898240	
[PZ99] J160654.4−241610	2.86	0.04	0.9	10.2	13900544	
[PZ99] J160703.9−191132	2.43	0.04	−6.2	9.5	13903104	
[PZ99] J160831.4−180241	2.87	0.04	8.6	14.6	13910784	
[PZ99] J160856.7−203346	3.35	0.04	−11.7	10.6	13898240	
[PZ99] J160930.3−210459	3.06	0.04	19.4	13.0	13911040	
[PZ99] J161302.7−225744	3.79	0.04	−7.3	10.0	13905920	
[PZ99] J161933.9−222828	3.63	0.04	−8.7	10.7	13903360	
RX J1548.0−2908	3.11	0.04	−4.2	13.3	13906688	
RX J1550.0−2312	2.91	0.04	0.9	17.7	13911296	
RX J1550.9−2534	5.02	0.04	4.8	18.7	13899264	
RX J1554.0−2920	3.17	0.04	3.6	9.5	13898752	
RX J1558.1−2405A	2.26	0.04	−46.3	37.6	13900032	
RX J1600.7−2343	0.95	0.04	−9.6	13.1	13909248	

Table 1
(Continued)

Source[a]	MIPS 24 μm[b]		MIPS 70 μm[c]		AORKEY	Flags
	S_ν (mJy)	σ (mJy)	S_ν (mJy)	σ (mJy)		
RX J1602.8−2401A	6.92	0.06	1.6	18.0	13900544	
RX J1603.6−2245	3.99	0.04	4.2	12.5	13902336	
SAO 183706	10.87	0.10	−17.8	25.0	13905664	
ScoPMS 13	3.08	0.04	−4.5	14.8	13899776	
ScoPMS 17	43.36	0.39	59.0	14.3	13901568	2, 4
ScoPMS 23	5.20	0.05	27.3	12.8	13902336	
ScoPMS 28	1.49	0.04	1.9	11.0	13905408	
ScoPMS 29	2.48	0.04	−2.8	9.6	13905408	
ScoPMS 31	334.60	3.00	296.7	11.5	13905408	
ScoPMS 32	0.98	0.04	−1.1	11.2	13909760	
ScoPMS 45	5.48	0.10	29.0	20.9	13910784	

Notes.
[a] Source names with the prefix [PZ99] and [PBB2002] are from Preibisch & Zinnecker (1999) and Preibisch et al. (2002), respectively.
[b] MIPS 24 μm photometry measured using a flux calibration factor of 0.0447 MJy sr^{-1}.
[c] MIPS 70 μm photometry measured using a flux calibration factor of 702 MJy sr^{-1}.
Flags: (1) 24 μm photometry is unreliable due to bright, extended nebulosity; (2) 24 μm photometry is unreliable due to nearby star; (3) Source is extended at 24 μm; (4) 70 μm photometry is unreliable due to contaminating source or nebulosity; (5) Contaminating source(s) subtracted before 70 μm photometry was measured; (6) 70 μm photometry measured on AOR 13903104.

(This table is also available in a machine-readable form in the online journal.)

ical result is consistent with the contamination anticipated from extragalactic source counts (Papovich et al. 2004). For each star in the sample, we computed the expected number of galaxies located within the full-width-at-half-maximum (FWHM) size (6″) of the MIPS 24 μm PRF that can produce a 30% photometric excess at 24 μm. (As described in Section 3.1, 30% is approximately the minimum excess detectable with these observations.) We find that ∼one star may be contaminated by an extragalactic source bright enough to produce such an excess.

A more significant level of contamination may arise from cirrus and nearby stars. We used both quantitative techniques and visual inspection of the images to identify such cases. First, we compared PRF photometry to aperture photometry obtained with a 6 pixel (1 pixel = 2.″55) aperture diameter, which is approximately 2.5 times the FWHM size of the MIPS 24 μm PRF. For 38 out of the 220 stars in the sample, the aperture photometry deviated from the PRF photometry by more than 10%. We chose 10% as the threshold since such deviations would impact the significance the 24 μm excesses identified in Section 3.1. Visual inspection of the images revealed that in the vast majority of cases, the difference between the aperture and PRF photometry is most likely due to low signal to noise since the aperture size is much larger than the optimal extraction size for relatively faint sources (Naylor 1998). The photometry was deemed questionable for six stars based on the presence of extended nebulosity (HIP 77840, HIP 78265, HIP 79404, and [PBB2002] USco J161052.4−193734) or because the 24 μm emission, while centered on the stellar position, is extended (HIP 77858 and HIP 80338). In addition, for the star ScoPMS 17, a known contaminating source is resolved in the 16 μm images (see Paper I) but is unresolved at 24 μm. These seven stars are flagged in Table 1.

2.2. *MIPS 70 μm*

MIPS 70 μm observations were obtained in photometry mode with an exposure time of 10 s and the small field size dither pattern. The number of cycles was fixed at 4 for all stars. MIPS 70 μm images were processed with SSC pipeline version S17 that removes the bias, subtracts a dark image, applies a flat field correction, and linearizes the pixel response. Individual BCD images were mosaicked with the Germanium Reprocessing Tools (GeRT) software package S14.0 version 1.1 developed at the SSC. A 40″ × 40″ region centered on the source position was excluded when computing the column and time filtering such that the filtering process is not biased by the presence of a bright source. Filtered images were formed into mosaics with MOPEX (Makovoz & Marleau 2005).

Aperture photometry was performed on the MIPS 70 μm mosaics with a custom version of IDLPHOT using an aperture radius of 16″ (4 pixels on the co-added images). The sky level was computed as the mean pixel value in a sky annulus that extended from 40″ to 60″. The aperture was centered on the expected stellar position computed from the world coordinate system keywords contained in the FITS image headers. No centroiding was performed since the signal-to-noise ratio of most 70 μm measurements is less than 3. Visual inspection of the 70 μm mosaics identified 19 images where a point source was located within the outer sky annulus or the aperture radius, but offset from the 2MASS stellar position by more than 4″. Before measuring the aperture photometry, a PRF was fitted to the apparent contaminating source and subtracted from the image using MOPEX.

The MIPS 70 μm photometry and internal uncertainties are presented in Table 1. Stars for which the 70 μm photometry was measured on PRF-subtracted images are marked in the table. The adopted calibration factor is 702.0 MJy sr^{-1}/(DN s^{-1}) with an uncertainty of 7% as reported on the SSC MIPS calibration web pages.[5]

Of the 220 stars in the sample, 15 have a 70 μm signal-to-noise ratio ⩾ 3. Photometry for two of these stars is compromised. ScoPMS 17 is contaminated by a nearby source resolved in the 16 μm images (see Paper I). HIP 80338 is surrounded

[5] http://ssc.spitzer.caltech.edu/mips/calib

Table 2
Normalized Flux Ratios.

Source	SpT	Ref SpT	A_V	Ratio[a] 24 μm	70 μm	σ(70 μm)	Excess? 24 μm	70 μm	Type
HD 142361	G3V	2	0.2	1.02	8.7	13.9			
HD 142987	G4	4	1.7	0.99	6.2	13.6			
HD 146516	G0IV	8	0.6	0.99	6.5	18.3			
HD 147810	G1	4	1.0	1.00	−8.3	9.8			
HD 149598	G0	4	0.7	1.13	18.5	36.2			
HIP 76071	B9V	2	0.3	0.98	−9.9	7.6			
HIP 76310	A0V	2	0.1	17.17	361.0	37.6	Y	Y	Debris
HIP 76633	B9V	2	0.3	1.30	12.1	9.1			
HIP 77457	A7IV	1	0.1	0.96	15.8	13.3			
HIP 77545	A2/3V	2	1.2	1.79	104.5	103.6	Y		Debris
HIP 77635	B1.5Vn	2	0.5	0.99	−2.1	3.3			
HIP 77815	A5V	2	0.7	1.04	0.0	10.9			
HIP 77840	B2.5Vn	2	0.4	0.88	−7.9	3.6			
HIP 77858	B5V	2	0.4	0.97	−1.0	4.7			
HIP 77859	B2V	2	0.6	1.68	−3.1	2.6	Y		Be
HIP 77900	B7V	1	0.2	0.98	−6.0	4.9			
HIP 77909	B8III/IV	2	0.1	0.99	1.5	5.8			
HIP 77911	B9V	2	0.3	9.64	159.4	17.2	Y	Y	Debris
HIP 77960	A4IV/V	2	0.6	1.02	−17.2	10.6			
HIP 78099	A0V	2	0.5	1.31	−15.7	7.4			
HIP 78104	B2IV/V	1	0.1	0.99	0.0	0.9			
HIP 78168	B3V	2	0.6	0.99	5.6	3.7			
HIP 78196	A0V	1	0.0	0.96	−1.3	6.8			
HIP 78207	B8Ia/Iab	2	0.1	4.36	12.4	1.8	Y	Y	Be
HIP 78233	F2/3IV/V	2	0.3	0.95	−2.9	13.1			
HIP 78246	B5V	2	0.2	0.99	4.1	3.2			
HIP 78265	B1V+B2V	2	0.2	1.07	0.2	3.0			
HIP 78483	G0V	1	0.4	0.98	8.3	18.3			
HIP 78494	A2mA7-F2	2	0.9	0.94	−11.0	9.3			
HIP 78530	B9V	2	0.5	1.07	1.5	12.7			
HIP 78549	B9.5V	2	0.4	1.03	−7.3	9.9			
HIP 78702	B9V	2	0.7	1.26	1.8	7.6			
HIP 78809	B9V	2	0.4	1.02	−10.2	14.4			
HIP 78820	B0.5V	2	0.7	1.06	0.9	0.3			
HIP 78847	A0V	2	0.5	1.00	5.1	9.6			
HIP 78877	B8V	2	0.1	1.03	−0.9	7.4			
HIP 78933	B1V	2	0.4	0.91	−0.3	1.3			
HIP 78956	B9.5V	2	0.6	1.55	1.0	10.4	Y		Debris
HIP 78963	A9V	1	0.4	0.96	15.4	15.7			
HIP 78968	B9V	2	0.5	1.84	−2.6	13.6	Y		Debris
HIP 78996	A9V	2	0.4	3.71	9.1	10.4	Y		Debris
HIP 79083	F3V	2	0.9	1.03	−2.0	5.0			
HIP 79097	F3V	2	0.3	1.00	−5.5	9.1			
HIP 79124	A0V	2	0.6	1.06	0.5	11.3			
HIP 79156	A0V	2	0.5	2.83	6.4	11.0	Y		Debris
HIP 79250	A3III/IV	2	0.2	1.29	−19.6	9.5			
HIP 79366	A3V	2	0.6	0.99	2.7	13.3			
HIP 79374	B2IV	2	0.9	0.95	0.5	0.9			
HIP 79392	A2IV	2	0.5	0.96	3.0	16.0			
HIP 79404	B2V	2	0.3	0.96	−6.9	3.1			
HIP 79410	B9V	2	0.6	3.77	6.9	10.2	Y		Debris
HIP 79439	B9V	2	0.6	1.99	25.5	12.2	Y		Debris
HIP 79462	G2V	2	0.3	1.51	−3.5	9.9	Y		Debris
HIP 79530	B6IV	2	0.4	0.97	1.3	5.3			
HIP 79606	F6	2	0.9	0.96	−9.8	11.7			
HIP 79643	F2	2	0.6	1.85	1.0	19.0	Y		Debris
HIP 79644	F5	2	0.8	0.93	−51.4	30.5			
HIP 79733	A1mA9-F2	1	1.4	1.00	−3.6	18.1			
HIP 79739	B8V	2	1.0	0.99	−14.4	18.1			
HIP 79771	B9V	2	1.1	0.97	−19.7	32.5			
HIP 79785	B9V	2	0.2	1.07	−3.4	6.9			
HIP 79860	A0V	1	0.3	1.03	−1.3	16.7			
HIP 79878	A0V	1	0.0	3.23	23.1	14.3	Y		Debris
HIP 79897	B9V	2	0.5	1.11	1.3	8.0			
HIP 80024	B9II/III	2	0.7	3.36	−8.7	65.4	Y		Debris

Table 2
(Continued)

Source	SpT	Ref	A_V	Ratio[a]			Excess?		Type
		SpT		24 μm	70 μm	σ(70 μm)	24 μm	70 μm	
HIP 80059	A7III/IV	2	0.5	0.99	−21.9	14.1			
HIP 80088	A9V	2	0.4	3.75	122.4	24.6	Y	Y	Debris
HIP 80112	B1III	2	1.2	0.95	2.7	6.4			
HIP 80130	A9V	2	0.6	1.04	2.3	12.7			
HIP 80311	A0V	1	1.0	0.86	10.1	50.5			
HIP 80324	A0V+A0V	1	0.0	1.03	5.4	11.3			
HIP 80338	B8II	2	2.3	1.42	62.9	17.2			
HIP 80493	B9V	1	0.9	1.01	4.2	18.3			
HIP 80896	F3V	1	0.0	0.97	30.4	12.1			
HIP 81266	B0V	1	0.3	1.17	−0.3	1.7			
HIP 82319	F3V	2	0.0	1.00	10.5	14.2			
HIP 82397	A3V	1	0.0	2.06	−4.9	12.8	Y		Debris
[PBB2002] USco J155624.8−222555	M4	7	1.7	22.18	110.8	82.8	Y		Primordial
[PBB2002] USco J155625.7−224027	M3	7	1.0	1.06	23.1	139.6			
[PBB2002] USco J155629.5−225657	M3	7	0.9	1.06	50.6	123.2			
[PBB2002] USco J155655.5−225839	M0	7	0.7	1.06	13.7	48.3			
[PBB2002] USco J155706.4−220606	M4	7	2.0	10.36	184.4	125.3	Y		Primordial
[PBB2002] USco J155729.9−225843	M4	7	1.4	11.21	433.6	219.2	Y		Primordial
[PBB2002] USco J155746.6−222919	M3	7	1.2	1.21	−6.2	153.2			
[PBB2002] USco J155829.8−231007	M3	7	1.3	28.99	76.5	120.7	Y		Primordial
[PBB2002] USco J155918.4−221042	M4	7	1.3	1.01	12.0	73.1			
[PBB2002] USco J160159.7−195219	M5	6	0.6	0.99	231.4	237.9			
[PBB2002] USco J160210.9−200749	M5	6	0.8	0.84	−224.6	301.4			
[PBB2002] USco J160222.4−195653	M3	6	1.2	1.05	99.6	132.4			
[PBB2002] USco J160226.2−200241	M5	6	0.3	0.90	21.7	166.3			
[PBB2002] USco J160245.4−193037	M5	6	1.1	0.97	−1.9	211.8			
[PBB2002] USco J160329.4−195503	M5	6	0.3	1.08	−2.0	213.6			
[PBB2002] USco J160341.8−200557	M2	6	0.9	1.03	−16.6	51.4			
[PBB2002] USco J160343.3−201531	M2	6	0.9	0.99	39.7	80.6			
[PBB2002] USco J160350.4−194121	M5	6	0.6	1.00	−34.4	108.8			
[PBB2002] USco J160357.9−194210	M2	6	1.7	22.45	219.3	86.7	Y		Primordial
[PBB2002] USco J160418.2−191055	M4	6	0.8	0.91	−253.6	198.3			
[PBB2002] USco J160428.4−190441	M3	6	1.0	1.00	−12.9	36.9			
[PBB2002] USco J160435.6−194830	M5	6	0.8	1.11	10.0	157.1			
[PBB2002] USco J160439.1−194245	M4	6	0.1	1.48	−33.1	141.9	Y		Debris
[PBB2002] USco J160449.9−203835	M5	6	0.7	1.07	−82.4	142.1			
[PBB2002] USco J160456.4−194045	M4	6	0.2	1.03	141.7	134.1			
[PBB2002] USco J160502.1−203507	M2	6	1.8	1.02	20.1	53.5			
[PBB2002] USco J160508.3−201531	M4	6	0.4	1.05	−73.6	57.0			
[PBB2002] USco J160516.1−193830	M4	6	0.7	0.89	−65.6	325.6			
[PBB2002] USco J160517.9−202420	M3	6	0.6	0.94	15.7	37.8			
[PBB2002] USco J160521.9−193602	M1	6	1.2	1.03	56.8	87.5			
[PBB2002] USco J160525.5−203539	M5	6	0.8	10.22	17.4	176.4	Y		Primordial
[PBB2002] USco J160528.5−201037	M1	6	1.0	1.06	−35.4	86.4			
[PBB2002] USco J160531.3−192623	M5	6	0.5	1.05	122.6	240.0			
[PBB2002] USco J160532.1−193315	M5	6	0.6	5.93	271.7	142.3	Y		Primordial
[PBB2002] USco J160545.4−202308	M2	6	2.2	26.32	298.4	113.8	Y		Primordial
[PBB2002] USco J160600.6−195711	M5	6	0.6	12.67	143.4	71.6	Y		Primordial
[PBB2002] USco J160611.9−193532	M5	6	1.5	0.97	52.2	181.1			
[PBB2002] USco J160619.3−192332	M5	6	0.6	0.85	−496.6	312.1			
[PBB2002] USco J160622.8−201124	M5	6	0.2	37.40	289.1	214.0	Y		Primordial
[PBB2002] USco J160628.7−200357	M5	6	0.0	1.05	153.5	105.6			
[PBB2002] USco J160643.8−190805	K6	6	1.8	5.29	46.7	33.6	Y		Primordial
[PBB2002] USco J160647.5−202232	M2	6	1.4	1.09	−54.9	70.1			
[PBB2002] USco J160702.1−201938	M5	6	1.0	14.53	112.6	187.0	Y		Primordial
[PBB2002] USco J160704.7−201555	M4	6	0.8	0.96	−59.3	296.9			
[PBB2002] USco J160707.7−192715	M2	6	1.8	1.18	−30.0	53.2			
[PBB2002] USco J160708.7−192733	M4	6	1.2	1.37	113.0	190.6	Y		Debris
[PBB2002] USco J160719.7−202055	M3	7	1.6	1.44	2.3	164.7	Y		Debris
[PBB2002] USco J160739.4−191747	M2	6	1.4	2.46	53.8	72.2	Y		Debris
[PBB2002] USco J160801.4−202741	K8	6	1.5	1.16	2.5	57.2			
[PBB2002] USco J160801.5−192757	M4	6	0.3	1.00	−24.1	56.4			
[PBB2002] USco J160802.4−202233	M5	6	0.7	1.02	20.4	129.0			
[PBB2002] USco J160804.3−194712	M4	6	0.0	0.84	−200.1	218.7			
[PBB2002] USco J160815.3−203811	M3	6	1.5	1.22	−206.0	140.2			

Table 2
(Continued)

Source	SpT	Ref	A_V	Ratio[a]			Excess?		Type
		SpT		24 μm	70 μm	σ(70 μm)	24 μm	70 μm	
[PBB2002] USco J160818.4−190059	M3	7	1.3	1.09	74.1	88.9			
[PBB2002] USco J160823.2−193001	K9	6	1.5	33.47	405.3	59.2	Y	Y	Primordial
[PBB2002] USco J160823.5−191131	M2	6	1.1	1.18	49.9	83.2			
[PBB2002] USco J160823.8−193551	M1	6	1.5	1.01	36.6	35.7			
[PBB2002] USco J160825.1−201224	M1	6	1.4	1.10	24.4	84.4			
[PBB2002] USco J160827.5−194904	M5	6	1.1	10.56	174.1	108.8	Y		Primordial
[PBB2002] USco J160843.1−190051	M4	6	1.1	1.01	−146.1	96.6			
[PBB2002] USco J160854.0−203417	M4	7	1.3	1.02	72.1	106.4			
[PBB2002] USco J160900.0−190836	M5	7	0.7	30.44	81.9	158.3	Y		Primordial
[PBB2002] USco J160900.7−190852	K9	6	0.8	101.78	834.3	93.0	Y	Y	Primordial
[PBB2002] USco J160903.9−193944	M4	6	0.7	0.88	24.4	105.9			
[PBB2002] USco J160904.0−193359	M4	7	1.6	1.00	13.7	149.9			
[PBB2002] USco J160913.4−194328	M3	6	1.4	0.99	−93.8	140.3			
[PBB2002] USco J160915.8−193706	M5	6	0.3	0.97	184.7	296.9			
[PBB2002] USco J160933.8−190456	M2	6	1.7	1.08	−142.9	89.8			
[PBB2002] USco J160946.4−193735	M1	6	1.6	1.07	13.8	76.6			
[PBB2002] USco J160953.6−175446	M3	7	1.9	22.76	341.5	252.8	Y		Primordial
[PBB2002] USco J160954.4−190654	M1	6	0.9	1.52	133.9	92.1	Y		Debris
[PBB2002] USco J160959.4−180009	M4	6	0.7	96.14	1006.3	156.3	Y	Y	Primordial
[PBB2002] USco J161010.4−194539	M3	6	1.0	1.09	74.4	109.7			
[PBB2002] USco J161011.0−194603	M5	7	0.5	2.02	58.2	302.8	Y		Debris
[PBB2002] USco J161014.7−191909	M3	6	0.9	1.50	24.0	91.5	Y		Debris
[PBB2002] USco J161021.5−194132	M3	7	1.6	1.12	−96.2	68.7			
[PBB2002] USco J161024.7−191407	M3	6	1.5	0.91	86.3	145.4			
[PBB2002] USco J161026.4−193950	M4	7	1.9	0.94	−38.2	111.6			
[PBB2002] USco J161031.9−191305	K7	6	1.1	1.04	16.3	62.2			
[PBB2002] USco J161052.4−193734	M3	7	2.3	1.96	78.0	92.8			
[PBB2002] USco J161115.3−175721	M1	6	1.6	17.71	41.1	27.1	Y		Primordial
[PBB2002] USco J161118.1−175728	M4	6	0.9	0.99	−61.3	48.0			
[PBB2002] USco J161420.2−190648	K5	7	1.8	40.07	201.1	21.6	Y	Y	Primordial
PPM 732705	G6	4	0.7	1.00	−17.3	29.2			
PPM 747651	G3	4	0.3	1.05	36.2	22.7			
PPM 747978	G3	4	0.7	0.94	3.0	50.6			
[PZ99] J153557.8−232405	K3:	5	0.7	0.90	5.5	66.9			
[PZ99] J154413.4−252258	M1	5	0.6	1.00	−49.0	52.9			
[PZ99] J155106.6−240218	M2	3	0.4	1.16	−103.2	73.5			
[PZ99] J155716.6−252918	M0	3	0.0	0.94	−12.6	48.9			
[PZ99] J155750.0−230508	M0	3	0.1	0.95	36.0	50.6			
[PZ99] J155812.7−232835	G2	3	0.4	2.72	54.7	75.0	Y		Debris
[PZ99] J155847.8−175800	K3	5	1.8	1.41	−46.9	32.1	Y		Debris
[PZ99] J160000.7−250941	G0	3	0.0	1.09	47.9	55.1			
[PZ99] J160013.3−241810	M0	3	0.6	1.50	−74.1	58.8	Y		Debris
[PZ99] J160031.3−202705	M1	3	1.0	0.98	−5.8	30.5			
[PZ99] J160042.8−212737	K7	3	0.8	1.01	6.5	37.5			
[PZ99] J160108.0−211318	M0	3	0.0	0.99	−0.9	26.6			
[PZ99] J160147.4−204945	M0	3	0.8	1.01	−7.8	26.6			
[PZ99] J160200.3−222123	M1	3	1.1	1.48	−31.2	32.5	Y		Debris
[PZ99] J160239.1−254208	K7	5	0.0	0.96	20.9	72.2			
[PZ99] J160251.2−240156	K4	3	0.6	1.22	−41.0	47.1			
[PZ99] J160354.9−203137	M0	3	0.9	0.99	−1.5	30.6			
[PZ99] J160357.6−203105	K5	3	0.9	33.16	176.9	21.3	Y	Y	Primordial
[PZ99] J160421.7−213028	K2	3	1.0	58.15	6204.3	623.8	Y	Y	Primordial
[PZ99] J160539.1−215230	M1	3	0.8	1.17	−10.4	61.7			
[PZ99] J160612.5−203647	K5	3	1.8	0.98	1.6	35.3			
[PZ99] J160654.4−241610	M3	5	0.0	0.93	3.0	33.4			
[PZ99] J160703.9−191132	M1	3	1.1	1.05	−23.7	36.4			
[PZ99] J160814.7−190833	K2	5	1.6	0.97	15.9	32.9			
[PZ99] J160831.4−180241	M0	5	0.1	1.06	28.1	47.7			
[PZ99] J160856.7−203346	K5	5	1.4	0.97	−32.7	29.7			
[PZ99] J160930.3−210459	M0	5	0.0	1.14	59.3	40.2			
[PZ99] J161302.7−225744	K4	5	2.3	1.00	−17.9	24.7			
[PZ99] J161318.6−221248	G9	5	0.9	0.98	−20.7	12.2			
[PZ99] J161329.3−231106	K1	5	2.0	1.03	28.8	25.4			
[PZ99] J161402.1−230101	G4	5	2.0	1.08	−50.0	33.4			
[PZ99] J161411.0−230536	K0	5	2.4	18.02	49.1	8.0	Y	Y	Primordial

Table 2
(Continued)

Source	SpT	Ref SpT	A_V	Ratio[a] 24 μm	70 μm	σ(70 μm)	Excess? 24 μm	70 μm	Type
[PZ99] J161459.2−275023	G5	5	1.0	1.57	85.8	81.1	Y		Debris
[PZ99] J161618.0−233947	G7	5	1.1	1.11	−25.8	24.6			
[PZ99] J161933.9−222828	K0	5	1.3	1.03	−22.3	27.5			
RX J1541.1−2656	G7	5	1.6	1.03	−152.6	56.6			
RX J1548.0−2908	G9	3	0.7	1.05	−12.7	39.8			
RX J1550.0−2312	M2	3	0.7	0.97	3.0	56.5			
RX J1550.9−2534	F9	3	0.2	0.91	8.8	34.7			
RX J1554.0−2920	M0	3	0.4	0.95	10.4	27.9			
RX J1558.1−2405A	K4	3	0.5	0.90	−190.8	156.1			
RX J1600.6−2159	G9	5	0.5	1.11	21.1	33.6			
RX J1600.7−2343	M2	3	0.5	0.90	−94.6	129.1			
RX J1602.8−2401A	K0	3	2.3	0.99	2.1	24.3			
RX J1603.6−2245	G9	3	1.2	1.00	9.8	29.1			
SAO 183706	G8e	4	1.7	1.04	−15.3	21.5			
ScoPMS 13	M1.5V	8	0.2	0.95	−13.7	44.9			
ScoPMS 17	M1V	8	0.7	14.68	12.7	3.3			
ScoPMS 21	K1IV	5	0.2	0.98	−21.0	67.3			
ScoPMS 23	K5IV	8	0.2	0.92	48.9	23.4			
ScoPMS 27	K2IV	5	0.2	0.94	12.6	19.7			
ScoPMS 28	M1V	8	0.7	0.96	11.6	68.5			
ScoPMS 29	M2V	8	0.7	1.02	−10.5	36.2			
ScoPMS 31	M0.5V	8	0.9	48.89	404.1	43.2	Y	Y	Primordial
ScoPMS 32	M3V	8	0.6	0.92	−10.9	106.6			
ScoPMS 45	K5IV	8	0.7	1.44	71.2	51.7	Y		Debris
ScoPMS 52	K0IV	8	1.3	0.97	35.3	24.6			

Note. [a] Ratio of the observed flux density to the photospheric value. The 24 μm ratios have an adopted uncertainty of 0.07.
References. (1) Houk 1982; (2) Houk & Smith-Moore 1988; (3) Kunkel 1999; (4) E. Mamajek 2009, private communication; (5) Preibisch et al. 1998; (6) Preibisch et al. 2001; (7) Preibisch et al. 2002; (8) Walter et al. 1994.

(This table is also available in a machine-readable form in the online journal.)

by nebulosity and it is ambiguous if the 70 μm emission is associated with the star. In the remainder of this paper, we do not include these two stars in analysis of the 70 μm data.

3. SOURCES WITH INFRARED EXCESSES

We now combine the 24 μm and 70 μm photometry for 220 Upper Sco members (i.e., 205 stars from this study, and 15 stars from FEPS; see Section 2) with 2MASS J and K_s (Skrutskie et al. 2006) and IRAC 4.5 μm (Paper I; Carpenter et al. 2008) photometry to identify stars with infrared excesses. All photometry was dereddened using the extinction law from Cardelli et al. (1989) assuming $R_V = 3.1$ for $\lambda \leqslant 2$ μm, the Chapman et al. (2009) reddening law for IRAC and MIPS 24 μm, and the reddening law compiled by Mathis (1990) for 70 μm. The visual extinction toward individual stars was obtained from the literature, or derived by us from published spectral types and optical/2MASS photometry following the general procedure described in Carpenter et al. (2008). The visual extinction is less than 2 mag for 97% of the stars, which implies a correction of less than 4% when dereddening the 24 μm photometry. The adopted spectral types and visual extinction for each star are listed in Table 2.

3.1. 24 μm Excesses

Figure 1 presents the 24 μm to 4.5 μm flux ratio ($\equiv R_{24/4.5}$) as a function of dereddened $J - K_s$ color for the Upper Sco sample. The $J - K_s$ color should represent the stellar photosphere for most sources since only two sources have an apparent K_s-band excess (Paper I). We chose to normalize the 24 μm photometry to the 4.5 μm band as a compromise between reducing the uncertainties in extinction corrections and the range of intrinsic photospheric colors (favoring longer wavelengths), and biasing the results due to weak emission from circumstellar dust (favoring shorter wavelengths). The locus of points with log $R_{24/4.5} \approx -1.4$ has flux ratios roughly consistent with the stellar photosphere for emission in the Rayleigh–Jeans limits. In practice, the value of $R_{24/4.5}$ varies systematically with $(J - K_s)_o$, indicating changes in the photospheric color with spectral type. A number of sources have values of $R_{24/4.5}$ that lie substantially above this locus. These sources include the 35 stars from Paper I that have an 8 μm and/or 16 μm excess as indicated by the black circles and crosses.

We adopted an iterative procedure to determine the locus of photospheric colors in the $R_{24/4.5}$ versus $J - K_s$ diagram. The trend between log($R_{24/4.5}$) and $(J - K_s)_o$ color was fitted using robust linear regression after first excluding the known 35 stars with 8 μm or 16 μm excesses and the seven stars flagged with suspect 24 μm photometry. Sources that deviated from the best-fit line by more than three times the dispersion of the residuals were removed, and the fit was repeated until no additional sources were excluded.

The best-fit relation is shown as the solid line in Figure 1. The dispersion about the best-fit line is $\sigma = 0.03$ dex (i.e., 7% of the photosphere) for the sources included in the fit. The largest deviation below the best-fit line is -2.5σ. Given the sample size of 220 stars, we expected only one source more discrepant

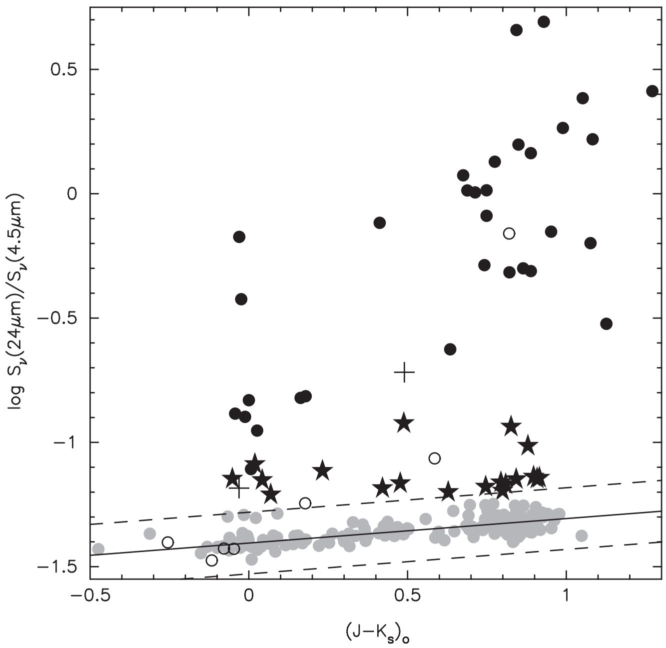

Figure 1. 24 μm to 4.5 μm flux density ratio ($R_{24/4.5}$) as a function of dereddened $J - K_s$ color. The solid line indicates the best-fit line ($\log R_{24/4.5} = 0.098\ (J - K_s)_o - 1.40$) to the main locus of points that is assumed to represent the stellar photosphere. The dashed lines indicate the $\pm 4\sigma$ limits about the fit ($\sigma = 0.03$ dex). Black circles indicate sources with an 8 μm or 16 μm excess from Paper I. Black stars are sources with detectable excesses at wavelengths $\geqslant 24$ μm, while gray circles indicate sources where the colors are consistent with photospheric emission. Sources with questionable photometry from nebulosity or a contaminating source are indicated by open circles, and known Be stars are marked by the crosses. The source [PBB2002] USco J161420.2−190648 is offscale on this plot at $(J - K_s)_o$, $R_{24/4.5} = 2.14, 0.27$.

than -2.5σ for Gaussian noise. The dispersion of 7% is larger than the median internal uncertainty (∼2%), suggesting that either the photometric precision is dominated by uncertainties not been quantified in our data reduction or that many of sources contain weak excesses. We conservatively adopt a 7% uncertainty on the $R_{24/4.5}$ ratio for all sources.

To identify stars that have a 24 μm excess, we required that the residuals exceed the photospheric color by $4\sigma = 0.12$ dex, or a 32% excess above the photosphere. We adopted 4σ as the cutoff since the dispersion in the residuals can vary by ∼0.003 dex depending on which stars are used in the fit. By choosing a 4σ cutoff, weak excesses are likely significant even if the dispersion is underestimated by 0.003 dex. In total, 54 stars have a value of $R_{24/4.5}$ that exceeds the stellar photosphere by more than 4σ and have reliable photometry. Of these 54 stars, 35 have an 8 μm and/or 16 μm excess, while 19 have a 24 μm excess only. These 19 sources are indicated by the filled stars in Figure 1. The sources with excesses only at 24 μm span the full range of spectral types and include four A/B-type stars, one F2 star, three G-type stars, two K-type stars, and nine M-type stars.

In addition to the checks described in Section 2.1, we visually re-inspected the 24 μm mosaics and the PRF subtracted images for the 54 stars with an infrared excess. Cutouts of the 24 μm images and PRF-subtracted images for these sources are presented in Figure 2. We identified seven stars where nebulosity or source confusion may compromise the photometry and create an apparent excess. Three stars (HIP 77545, HIP 80024, and ScoPMS 45) are located in regions of extended nebulosity, although the observed PRF is point-like. Four other stars ([PBB2002] USco J155729.9−225843, [PBB2002] USco J160532.1−193315, [PBB2002] USco J160708.7−192733, and [PBB2002] USco J160900.0−190836) have a neighboring source within ∼20″. We have re-reduced the data for these sources using smaller sky annuli for the PRF fit, and examined various aperture measures. In each case, the infrared excess is robust to these variations in the data reduction. Also, in four of the seven sources, the excess is confirmed by IRAC 8 μm or IRS 16 μm photometry, where confusion and nebulosity are less of a concern. We therefore classify these seven stars as having an 24 μm excess, but we note that the excesses around HIP 77545, [PBB2002] USco J160708.7−192733, and ScoPMS 45 are detected only at 24 μm and are otherwise unconfirmed.

The ratio of the observed 24 μm flux density to the photospheric value was estimated from the observed photometry and the expected stellar colors. If a source does not have an excess in the 4.5 μm or 8 μm bands (see Paper I), the observed-to-photospheric 24 μm ratio was computed from the observed $R_{24/4.5}$ ratio and the photospheric value determined from the $R_{24/4.5}$ vs. $(J - K_s)_o$ relation shown in Figure 1. Otherwise, the 24 μm photospheric flux density was bootstrapped from the K_s-band photometry (or J-band if a K_s excess is present) using empirical relations between spectral type and $J - K_s$ color (Paper I; Dahm & Carpenter 2009), spectral type and $K{-}M$ color[6] compiled by Kenyon & Hartmann (1995), and the $R_{24/4.5}$ versus $(J - K_s)_o$ relation. Table 2 lists the ratio of the observed-to-photospheric 24 μm flux densities for each star.

3.2. 70 μm Excesses

The photospheric flux density at 70 μm was estimated from the 24 μm flux density by assuming that the stellar emission is in the Rayleigh–Jeans limit (i.e., $S_\nu \propto \nu^2$). If the source has a known 24 μm excess, the photospheric 24 μm flux density was estimated as described in Section 3.1. Otherwise, the observed 24 μm flux density was used.

Figure 3 presents a histogram of the measured signal-to-noise ratio for the observed 70 μm infrared excess above the stellar photosphere. The detected 70 μm flux density from the B0.5 star HIP 78820 is consistent with the photospheric emission. Excluding the two stars where the measured 70 μm flux density is suspect (see Section 2.2), 12 stars have an apparent 70 μm excess greater than 3σ. Sources with 70 μm excesses include four A/B stars, six K stars, and two M stars. All 12 of these stars also have a 24 μm excess, as well as an 8 μm or 16 μm excess identified in Paper I.

4. NATURE OF THE DISK CANDIDATES

The circumstellar dust producing the infrared excesses observed in Upper Sco may originate from either a "primordial" or "debris" disk. Conceptually, primordial disks contain copious amounts of gas and dust that are remnants of the star formation process, while debris disks are gas-poor systems created by the collisional shattering of planetesimals.

Distinguishing primordial from debris dust is difficult observationally at an age of 5 Myr. The inner portion of most primordial disks are optically thin by this age as traced by 3–10 μm observations (Mamajek et al. 2004; Hernández et al.

[6] We compared the empirical $K{-}M$ colors versus the model $K - [4.5]$ colors from the Stellar Performance Estimation Tool (STAR-PET) available on the *Spitzer* Web site. Between spectral types of A0 and G5, the maximum difference between the two colors is 0.03 mag. For M0 stars, the color difference is 0.15 mag. A comparison with the observational data indicates that the $K{-}M$ colors provide a better match to the data.

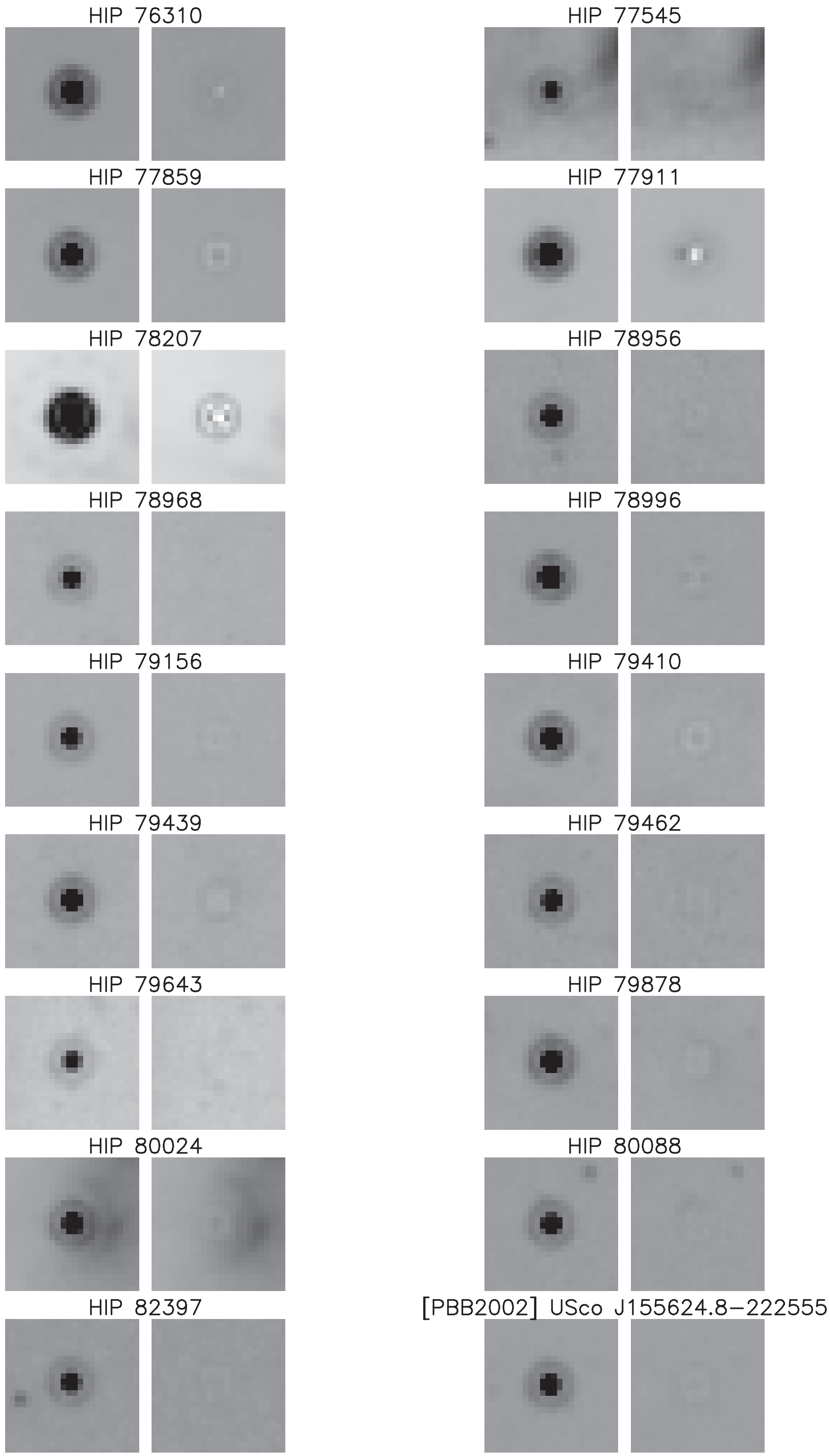

Figure 2. 24 μm images for the 54 Upper Sco stars with a 24 μm excesses. The left panel for each star shows a $1' \times 1'$ region centered on the stellar position. The right panel shows the PRF-subtracted image, where all identified stars in the field of view have been fitted and removed. All images are displayed in a logarithmic scale.

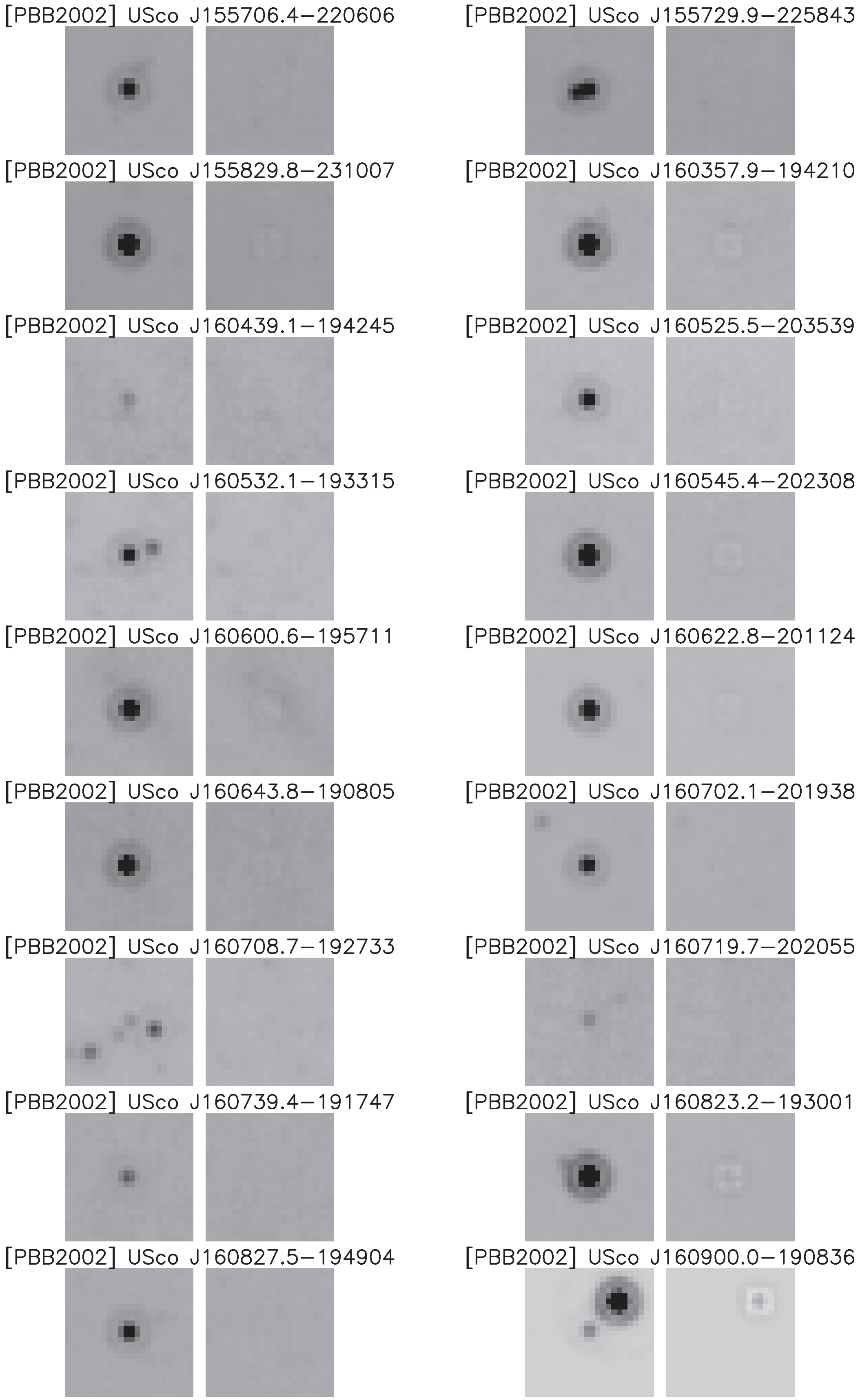

Figure 2. (Continued)

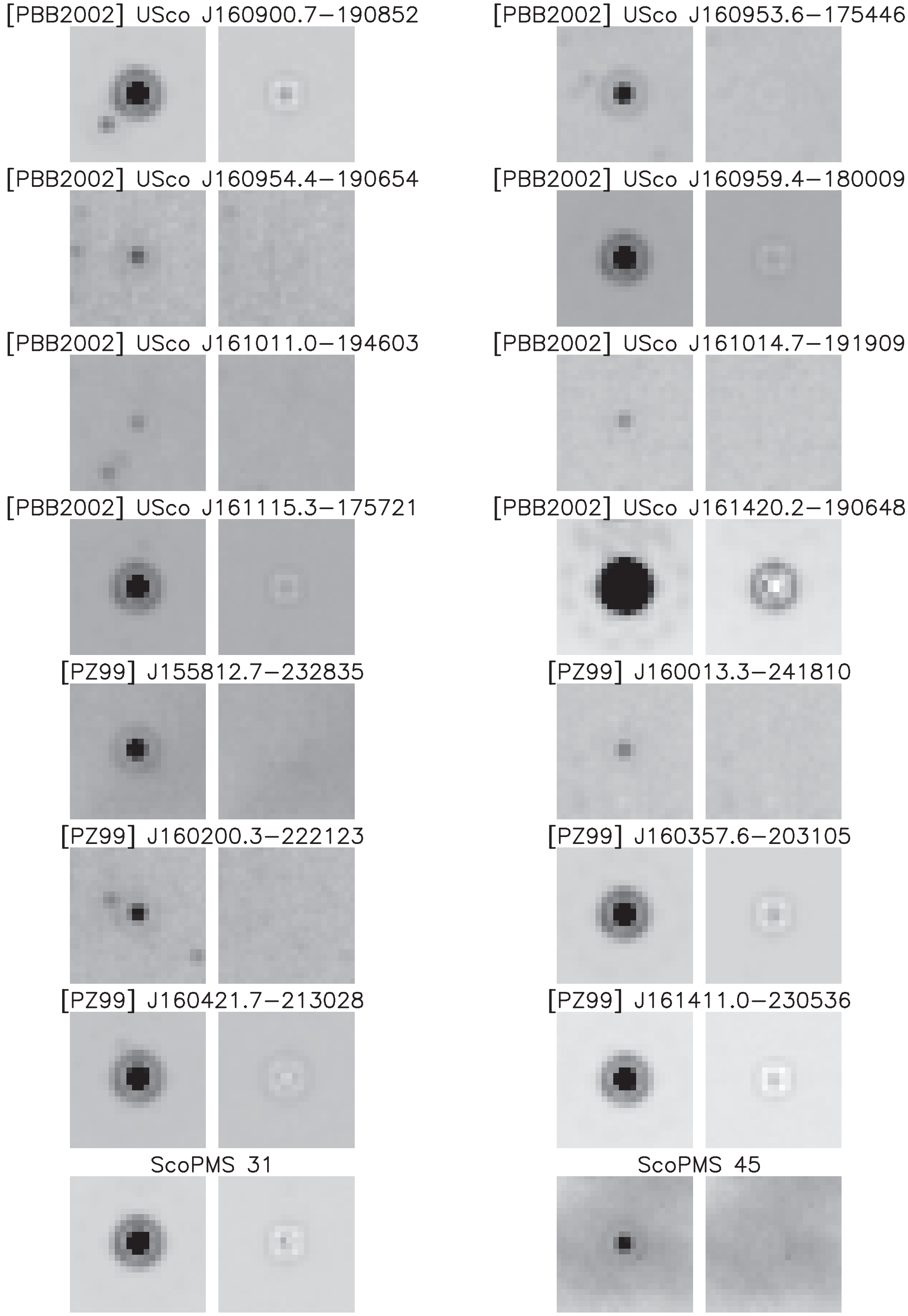

Figure 2. (Continued)

2007), but the state of the outer disk as traced by wavelengths longer than 24 μm remain poorly characterized. The classic argument to support the debris interpretation is that radiative and collisional processes can deplete the dust on timescales much shorter than the stellar age assuming the disk is gas poor (Backman & Paresce 1993). Therefore, the dust must be replenished continuously, presumably from a collisional cascade, to explain the observed infrared excesses. This argument assumes that gas drag is negligible, which can circularize the orbits of the dust grains and reduce the frequency of destructive collisions. Models by Takeuchi & Artymowicz (2001) indicate that 10 $M_\oplus$ of gas distributed radially over ~100 AU can prolong the lifetime of grains around A-type stars to a couple of million years, which is comparable to the age of Upper Sco.

Unfortunately, observations of the gas component are not available for most of the Upper Sco sample. Several stars in Upper Sco have strong Hα emission lines that suggest gas accretion is present, although most stars do not appear to be

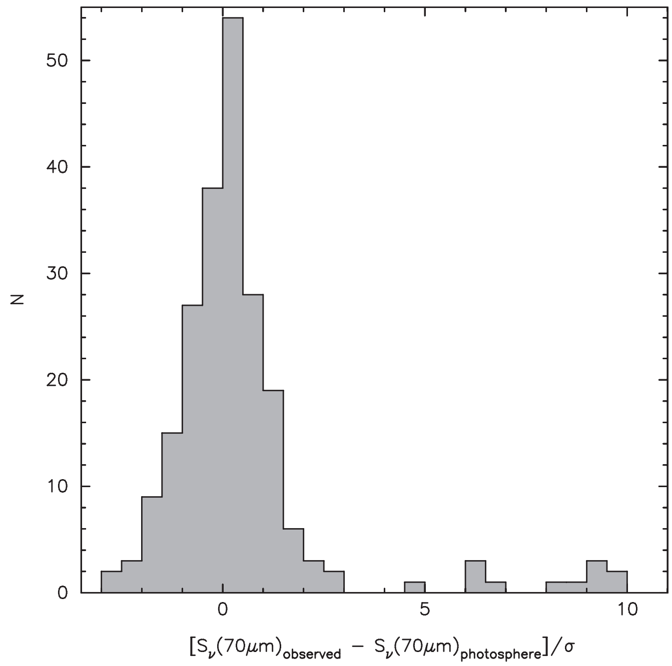

Figure 3. Histogram of the signal-to-noise ratio for the observed 70 μm excess above the stellar photosphere. The histogram excludes two stars (ScoPMS 17 and HIP 80338) for which the 70 μm photometry is suspect (see Section 2.2). Sources were identified as having a significant excess if the observed 70 μm flux density exceeded the photospheric flux density by $\geqslant 3\sigma$.

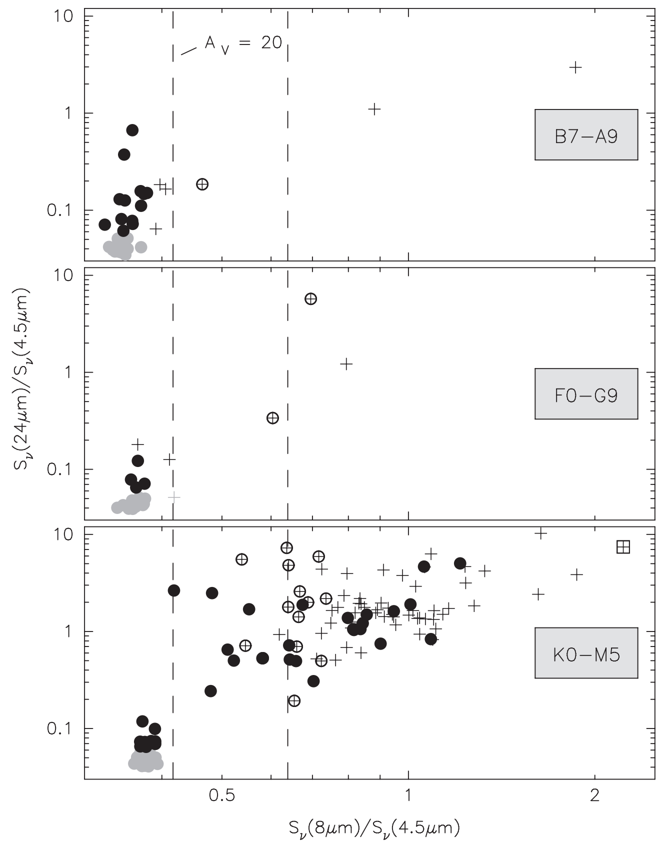

Figure 4. The dereddened 24 μm to 4.5 μm flux ratio as a function of the dereddened 8 μm to 4.5 μm flux ratio for B7-A9 stars (top), F0-G9 stars (middle), and K0-M5 stars (bottom). Filled circles represent stars in Upper Sco, and crosses indicate stars in IC 348 that have a 24 μm detection (Lada et al. 2006). Black symbols indicate stars with an infrared excess at 24 μm (excluding two Be stars), and gray symbols indicate stars that lack a 24 μm excess. Crosses bounded by circles and squares are stars in IC 348 that have been classified by Lada et al. (2006) as "anemic" or "flat" based on the slope of the SED in the *Spitzer* IRAC bands. The dashed lines indicate the range of slopes ($\alpha = -2.56$ to 1.80) used to define anemic disks ($\alpha = d\log(\nu S_\nu)/d\log(\nu)$). A few anemic disks lie outside these boundaries since the actual slopes were computed using all four IRAC bands. A G0 star in IC 348 is offscale at (6.4, 4.8).

accreting detectable levels of material (Dahm & Carpenter 2009). Yet even these observations only trace gas in the inner disk and are not direct diagnostics of the total gas surface density. Extensive surveys for gas in 5–100 Myr stars have been presented in other studies that are designed to trace the gas over a range of orbital radii (Zuckerman et al. 1995; Najita & Williams 2005; Pascucci et al. 2006). Even these observations, though, cannot rule out that gas drag has a significant influence on the dust dynamics.

Given the lack of observations of the gas component, we rely on distinctions in the spectral energy distributions (SEDs) between stars in Upper Sco and other known sources to identify potential debris systems. In Paper I, we compared the SEDs of the Upper Sco sample between 2 and 16 μm with Herbig Ae/Be stars and classical T Tauri stars. We suggested that the infrared excesses around the B/A stars represent debris systems, while the K/M stars with 8 μm and 16 μm excesses originate from optically thick disks, albeit with suppressed levels of mid-infrared emission relative to a typical classical T Tauri star in Taurus. The 24 μm photometry and IRS spectra for a subset of these sources support these conclusions (Dahm & Carpenter 2009).

With the discovery of 19 additional disks in Upper Sco from the 24 μm photometric survey, we further investigate the range of disk characteristics. Figure 4 plots the 24 μm to 4.5 μm flux ratio versus the 8 μm to 4.5 μm flux ratio for stars in Upper Sco with (solid black circles) and without (gray circles) 24 μm excesses. Qualitatively, a dichotomy is present in the excess characteristics. One population, present only for stars with spectral types later than K0, has both 8 μm and 24 μm excesses, and has colors similar to stars surrounded by optically thick, primordial disks (Paper I; Dahm & Carpenter 2009).

The second population of 24 μm excess sources, present among all spectral types, has weak or no detectable 8 μm excesses. Among the K0-M5 stars, the magnitude of the 24 μm excess for this second population is less than the 24 μm excess found in any of the sources with both 8 μm and 24 μm excesses. If we assume the dust is isothermal, a lower limit to the dust temperature obtained from the 24 μm excess and the 70 μm upper limit is ~53 K for blackbody emission. The upper limit to the fractional dust luminosity for this dust temperature and a stellar temperature of 4000 K is $\sim 10^{-4}$. This fractional luminosity is orders of magnitude lower than that found from optically thick disks around classical T Tauri stars.

With the large number of *Spitzer* surveys of star-forming regions, the primordial disk classification has been refined to include "transitional" (Strom et al. 1989), "pre-transitional" (Espaillat et al. 2007), "evolved" (Hernández et al. 2007), "homologously depleted" (Currie et al. 2009), and "anemic" (Lada et al. 2006) designations. Each of these disk types is characterized by reduced levels of emission at wavelengths $\lesssim$ 10 μm relative to classical T Tauri stars. The reduced infrared emission can be caused by a number of processes, including dynamical clearing of dust by a companion, grain growth, and disk settling.

To compare the characteristics of the Upper Sco sample with anemic disks, Figure 4 shows the infrared colors from Lada et al.

(2006; see also Currie & Kenyon 2009) for confirmed members of IC 348 (see Luhman et al. 2003). IC 348 was chosen for this comparison since the cluster contains a similar range of spectral types as Upper Sco, and was used to define anemic disks. One limitation, however, is that the IC 348 observations detected the photosphere at 24 μm for A-type stars only, and are not sensitive to the weak 24 μm excesses observed around the later type stars in Upper Sco. The vertical dashed lines show the range of slopes in the IRAC bands used to define anemic disks, while an 8 μm to 4.5 μm flux ratio greater than 0.64 would be classified as an optically thick disk (Lada et al. 2006). None of the B/A/F/G stars in Upper Sco with an infrared excess would be classified with anemic or optically thick disk based on these criteria. The circled crosses in Figure 4 show the actual stars in IC 348 that were identified by Lada et al. (2006) to have anemic disks based on the fitted slope to all four IRAC bands. For B7-A9 (top panel in Figure 4) and F/G spectral types (middle panel), the anemic and optically thick disks in IC 348 have larger 8 μm excesses than any of the sources in Upper Sco. The 24 μm excesses also tend to be larger in IC 348, although the distribution overlaps significantly with Upper Sco.

The Upper Sco sources with excesses detectable at 24 μm only also do not fit the operating definition of transitional disks. Transitional disks are noted by a lack of continuum excesses at wavelengths $\lesssim 10\ \mu$m, but retain excesses at longer wavelengths comparable in strength to classical T Tauri stars. As shown in Figure 4, the K/M stars in Upper Sco with excesses at 24 μm only have systematically lower 24 μm excesses than the stars with optically thick disks. This does not necessarily indicate that the dust is debris, as a spectrum of inner hole sizes may exist, and the weak 24 μm excesses may simply indicate a larger inner hole is present in the disks around the Upper Sco sample. While none of these systems were detected at 70 μm, most primordial disks were not detected at 70 μm either. Therefore, the 70 μm limits for the weaker 24 μm excesses are insufficient to rule out a cold, optically thick outer disk.

In summary, the above discussion suggests that Upper Sco contains two populations of excess sources. The late-type stars with strong 8 μm and 24 μm excesses plausibly have primordial disks based on the presence of accretion signatures in a few stars, and a similarity in the infrared colors of young stars surrounded by optically thick disks (Paper I; Dahm & Carpenter 2009). Many of these sources have infrared colors similar to "anemic" disks (Lada et al. 2006). The origin of the dust producing the weak 24 μm excesses remains uncertain, but these disks are likely not a simple extension of the transitional or anemic disk designations. Without additional observations, we can only assume that these disks are gas poor and the dust originates from a debris disk, but we cannot rule out that the dust is remnant primordial material.

In Table 2, we classify each of the disks candidates as primordial, debris, or Be. A summary of the classifications by spectral type is provided in Table 3. Primordial disks were assigned to K/M-type stars that have 8 μm and 16 μm excesses since their infrared excess characteristics are similar to optically thick disks (see also Dahm & Carpenter 2009, Paper I). Two stars (HIP 77859 and HIP 78207) have prominent hydrogen emissions in optical spectra and have been identified as classical Be stars (Crampton 1968; Jaschek et al. 1964); the observed infrared excess may originate from free–free emission in an ionized gas disk (Porter & Rivinius 2003). The remaining sources with infrared excesses were classified as debris disks given the relatively weak excesses at 8, 16, or 24 μm. As noted

Table 3
Disk Types in Upper Sco

Spt	N(stars)	N(disks)		
		Be	Debris	Primordial
B	37	2	6	0
A	25	0	7	0
F	9	0	1	0
G	21	0	3	0
K	27	0	2	7
M	101	0	9	17
Total	220	2	28	24

in Paper I, optically thick primordial disks are present in 19% of the K/M stars in the Upper Sco sample, and in none of the B, A, F, and G stars. Debris disks are detected around all spectral types, with percentages of 9% for K/M stars, 13% of F/G stars, and 28% of B/A stars.

5. PROPERTIES OF THE DEBRIS DISKS

A direct comparison of the debris fractions between early- and late-type stars does not necessarily inform how the frequency of disks varies with spectral type. Since observations at a given wavelength probe dust at smaller orbital radii around cooler stars for a fixed grain size, the low 24 μm debris fraction around K/M stars relative to A-stars may simply reflect that the debris is located at large orbital radii and is too cool to detect in the 24 μm band.

Nominally, the orbital radius of the debris can be inferred from the dust temperature. This is possible only for the debris disks around the B/A stars where the debris emission is detected at two or more wavelengths. For the F/G/K/M stars, the debris emission is detected only at 24 μm, and a broad range of temperatures and radii can fit the single photometric point. We instead pose the question: can the debris properties inferred around the B/A stars also explain the debris emission observed around the later spectral types?

The emitted radiation from a debris disk varies with spectral type due to differences in stellar heating and radiative "blowout" of small grains (Plavchan et al. 2009). To compare the debris properties between spectral types in a self-consistent manner, we assume the debris is located in a narrow ring at an orbital radius R. The particles follow a power-law size distribution, $n(a)$, between grain radii $a_{\min}$ and $a_{\max}$ such that

$$n(a) = N_o \left(\frac{a}{a_{\min}}\right)^{\alpha}, \quad (1)$$

where N_o is the normalization constant that effectively determines the total grain surface area. The power-law exponent is fixed at $\alpha = -3.5$ as appropriate for an infinite collisional cascade without binary conditions on the minimum and maximum particle size (Dohnanyi 1969). In practice, the maximum grain size was fixed at $a_{\max} = 1000\ \mu$m, and the minimum grain size ($a_{\min}$) was set to either the blowout size or 0.05 μm, whichever was larger. Excluding smaller grains does not impact the results significantly since such small grains are inefficient emitters at 24 μm.

The grain sizes that will remain gravitationally bound to a star were assessed by balancing the stellar gravitational force (F_g) against repulsive forces from radiation (F_{pr}) and stellar winds (F_{sw}). The ratio of these forces (β) for a particle of radius a is given by

$$\beta(a) = \frac{F_{\rm pr} + F_{\rm sw}}{F_{\rm g}} = \frac{3L_*(Q_{\rm rad}(a) + Q_{\rm sw}(a)\,\dot{M}_{\rm sw}\,v_{\rm sw}\,c/\,L_*)}{16\pi GM_*\rho ca}, \quad (2)$$

where L_* is the stellar luminosity, $\dot{M}_{\rm sw}$ is the stellar mass loss rate, $v_{\rm sw}$ is the stellar wind velocity, $Q_{\rm rad}(a)$ is the particle cross section to radiation in units of the geometric cross section, $Q_{\rm sw}(a)$ is the analogous cross section for stellar winds, and ρ is the grain density (Burns et al. 1979; Gustafson 1994; Strubbe & Chiang 2006). Assuming the disk is optically thin, particles for which $\beta < 0.5$ remain gravitationally bound to the star, while particles with $\beta > 0.5$ are ejected. The stellar wind velocity was set to the escape velocity ($v_{\rm sw} = \sqrt{2GM_*/R_*}$). The stellar mass loss rate is uncertain by orders of magnitude for these young ages across all spectral types. The force from stellar winds is negligible for the grain radii considered here unless the mass loss rate is $\gtrsim$ 1000 times the solar value (Plavchan et al. 2005; Strubbe & Chiang 2006). We assume $\dot{M}_{\rm sw} = 2 \times 10^{-14}\,M_\odot$ yr^{-1}, which corresponds to the solar mass loss rate (Wood 2004), and that $Q_{\rm sw}(a) = 1$. The dust emission was computed using optical constants for astronomical silicates (Weingartner & Draine 2001) and assuming $\rho = 2.7$ g cm^{-3}. Stellar photospheres were approximated as blackbodies.

Given the debris disk model, we can normalize the two free model parameters (R and $N_{\rm o}$) using the nine B/A stars in Upper Sco that have both 16 μm and 24 μm excesses. The ratio of the 16 μm to 24 μm excess flux densities determines the orbital radius of the dust, R. The ratio varies between 2.8 and 10.0 with a median value of 3.8, which leads to an orbital radius between 9 AU and 40 AU with a median of 15 AU. Given the orbital radius, the total surface area of dust contained in particles gravitationally bound to the star ($\beta < 0.5$) is set by the magnitude of the 24 μm emission given the inferred orbital radius, which determines $N_{\rm o}$ in Equation (1). The 24 μm excess for all 13 B/A stars with debris disks varies between 0.5 and 16 times the photosphere, with a median of $\sim$ 2.

To compute the excess emission around stars of other spectral types, stellar properties (mass, luminosity, and temperature) were obtained from the 5 Myr pre-main-sequence isochrone of Siess et al. (2000) for solar metallicity. The orbital radius (R) and the size distribution ($N_{\rm o}$) of the dust were fixed to that inferred around the B/A stars. However, for a given L_* and M_*, only grains with $\beta < 0.5$ were included in the calculations of the debris emission. Therefore, even though $N_{\rm o}$ is fixed, the total dust surface area is larger for later spectral types since the radiation blowout size is smaller. The ratio of the expected dust emission excess to the photosphere was computed in this manner for stars between masses of 0.1 $M_\odot$ and 7 $M_\odot$.

Figure 5 presents the results of the calculations for 16 μm and 24 μm excesses. The shape of the model curves reflects variations in stellar heating and the minimum grain size present in the disk. The dust surface area decreases toward early spectral types and tends to reduce the dust emission, which is compensated by warmer dust temperatures. The 24 μm excess relative to the photosphere (hereafter referred to as the relative 24 μm excess) peaks at a spectral type of $\sim$ B7 ($J - K_{\rm s} \approx -0.06$), and declines toward more luminous stars as more small grains are ejected by radiation pressure. Toward later spectral types, the relative 24 μm excess at first declines despite the increased surface area since the dust temperature decreases with lower stellar heating. However, at a color of $J - K_{\rm s} \approx 0.2$ ($\sim$ F0 star), the blowout particle radius is $\sim 5\mu$m, and the dust temperatures are warmer than expected based on blackbody radiation. Combined with the increased surface area of these smaller grains, the normalized 24 μm excess ratio plateaus toward cooler stars until a stellar color of $J - K_{\rm s} \approx 0.8$ ($\sim$ M0 star). At this point the blowout size is less than 0.1 μm and these small grains emit inefficiently at 24 μm. Therefore the additional

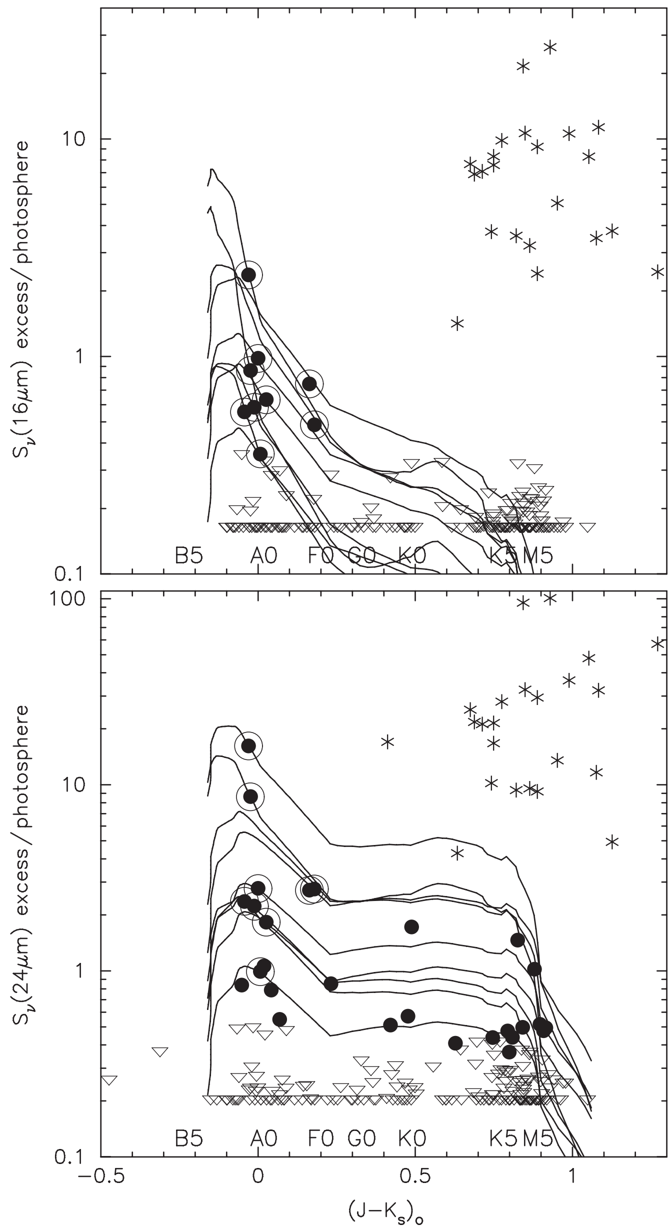

Figure 5. 16 μm (top panel) and 24 μm (bottom panel) excess in Upper Sco normalized by the photospheric emission as a function of the dereddened $J - K_{\rm s}$ color. Symbols indicate debris (filled circles) and primordial (asterisks) disks. Triangles indicate the 3σ upper limits for stars without detected excesses. Be stars and sources with contaminated photometry have been omitted. The solid curves show the emission from model debris disks with a power-law distribution of particle sizes at a given orbital radius. The models were normalized to the debris properties around B/A stars, and computed around stars of various temperatures after factoring differences in stellar heating and radiation blowout size. Open circles indicate the nine B/A stars used to normalize the models. See text for explanation of model behavior as a function of photospheric color. The results indicate that the magnitude of the 16 μm and 24 μm excess around the debris disks can be explained by planetesimals belts that have a similar range of orbital radii across all spectral types.

surface area from small grains does not appreciably increase the amount of infrared excess. The 16 μm curves exhibit similar behavior, but fall more steeply toward later spectral types since the dust emission is further into the Wien regime and more sensitive to the dust temperature.

Figure 5 shows that if the only variation in the debris properties is the blowout size and stellar heating, the 24 μm excess relative to the photosphere will be $\sim$2 times higher around $\sim$A0 stars compared to F0-M0 stars at an age of 5 Myr. The relative 24 μm excess decreases rapidly toward stars earlier than B7 and later than M0. Qualitatively, the range of relative 24 μm excesses around the F/G/K/M-type stars are consistent with the extrapolation of the excesses around the B/A stars based on this model. At 16 μm, the relative photometric excess falls sharply with later spectral types and 16 μm excesses would be undetectable toward the later type stars. This model is consistent with the lack of 16 μm excesses from debris in F/G/K/M stars (Paper I). We conclude that is not necessary to invoke systematic differences in the radial distribution of dust with spectral type to explain the range of observed 16 μm and 24 μm excesses.

6. EVOLUTION OF DEBRIS EMISSION

Variations in the debris luminosity with stellar age provide a means to investigate the evolution of planetesimal belts and potentially the formation of planetary systems. Dominik & Decin (2003; see also Wyatt et al. 2007b) suggested that the evolution of debris emission can be explained by quasi-steady-state collisional equilibrium of planetesimals distributed in a narrow ring. One limitation of this model is that it does not prescribe a physical mechanism to initiate the collisional cascade. In a series of papers, Kenyon & Bromley (2008; and references therein) presented a model that follows both the collisional growth of planets and the onset of debris production. They show that the debris disk initially has a low luminosity when planets are still in the formative stages. When the collisional growth produces $\sim$ 2000 km size bodies, the resulting gravitational interactions excite planetesimal collisions that leads to dramatically increased debris luminosity. The timescale to form a 2000 km body increases with the orbital radius, thereby producing a "wave" of debris production in time that propagates from the inner disk outward.

A prediction of the Kenyon & Bromley model is that the debris luminosity initially increases with time, and then declines once the wave of debris production has propagated outward through the disk on a dynamical timescale. For a debris disk that extends between 30 and 150 AU, the debris emission will peak at an age of $\sim$5–30 Myr, with faster timescales for higher mass stars given a fixed disk mass. A decline in debris luminosity for ages older than $\sim$20 Myr has been observed in a number of studies and seems firmly established by the data (Habing et al. 2001; Decin et al. 2003; Rieke et al. 2005; Siegler et al. 2007; Carpenter et al. 2009). Hernández et al. (2006) and Currie et al. (2008a) further suggest that the 24 μm excess around A/F stars increases from an age of $\sim$5 Myr and peaks around 10–15 Myr. If verified, this initial increase in 24 μm debris luminosity may signify the onset of planetesimal stirring in debris disks.

The Upper Sco observations presented here provide an important data point to re-evaluate the trends at young ages since few surveys for debris disks are available for younger stars than 10 Myr. As described in the Appendix, we have compiled the results from a number of *Spitzer* 24 μm surveys for comparison to Upper Sco. Similar compilations have appeared in Gaspar et al. (2009), Rebull et al. (2008), Currie et al. (2008a), and Siegler et al. (2007) among others. The compiled surveys include clusters and associations between ages of 2 and 757 Myr, and field stars between ages of 3 and 5000 Myr. The young associations and clusters that have been surveyed previously are either sparsely populated with only $\sim$20 members (η Cha, Gautier et al. 2008; TW Hydra moving group, Low et al. 2005) or are at large distances such that *Spitzer* is sensitive to the stellar photosphere for only A-type stars or earlier (IC 348, Lada et al. 2006; σ Ori, Hernández et al. 2007; Orion OB1a and OB1b, Hernández et al. 2006; NGC 2262, Currie et al. 2008b).

The spectral-type bins were selected to be B7-A9, F0-F9, and G0-K5, which correspond to the spectral-type ranges where numerous *Spitzer* studies exist (see Appendix). Stars earlier than B7 were omitted since they are fewer in number, and as shown in Section 5, the debris luminosity may be depressed by radiative blowout of the smallest grains. Stars later than K5 are omitted since most *Spitzer* surveys of young clusters and associations were insensitive to the stellar photosphere for K/M stars. The relationship between the empirical variable of spectral-type and the physical variables stellar mass and luminosity, which dictate debris disk properties, will be discussed in Section 6.3.

As discussed in Section 4, we are faced with the ambiguity of distinguishing if the "anemic," "evolved," and "transitional" disks are debris or primordial systems. We proceed by an entirely observational definition. The disk around HR 4796A is commonly assumed to be debris in nature. The ratio of the observed 24 μm emission to the photosphere for this disk is 97, which is one of the largest relative 24 μm excesses known. We therefore assume that any B/A/F star with an "anemic," "evolved," or "transitional" classification and has an observed-to-photospheric 24 μm flux ratio of $\leqslant$ 100 is a debris disk, while more luminous systems are primordial disks. For G- and K-type stars, we use a limit of 5 based on the division shown in Figure 4. These divisions are arbitrary and not physically motivated. Changing these boundaries by even a factor of 2 has no substantial impact on our conclusions.

6.1. 24 μm Excess Fraction

We first examine how the fraction of stars with 24 μm infrared excesses varies with age. We consider two different thresholds to identify infrared excess: 32% to incorporate the largest number of studies, and 15% to increase sensitivity to fainter disks. The adopted thresholds for each survey are listed in the Appendix. Any surveys with sensitivity limits larger than these thresholds were omitted from the appropriate plot. The excess fraction is defined as the ratio of the number of debris disks to the total number of stars (i.e., optically thick disks, debris disks, Be stars, and non-excess stars). Stars were omitted from the statistics if the original study noted that the photometry was contaminated (e.g., nebulosity, nearby bright star) such that it was not possible to determine if the star has an excess or not.

Figure 6 presents the excess fraction for the three spectral-type groupings. For G0-K5 stars, the 24 μm excess fraction in Upper Sco is 11% (6/54) at the 32% detection threshold, which is indistinguishable from the excess fraction (6/56) observed for 10–30 Myr G0-K5 stars. This result is consistent with the FEPS program, which found that the excess fraction for solar-type stars is roughly constant for ages $\lesssim$ 300 Myr (Meyer et al. 2008; Carpenter et al. 2009).

Other studies have found that the debris disk fraction for solar-type stars can be as high as 40%–45% between ages of 3 and 30 Myr (Siegler et al. 2007; Gaspar et al. 2009). The difference

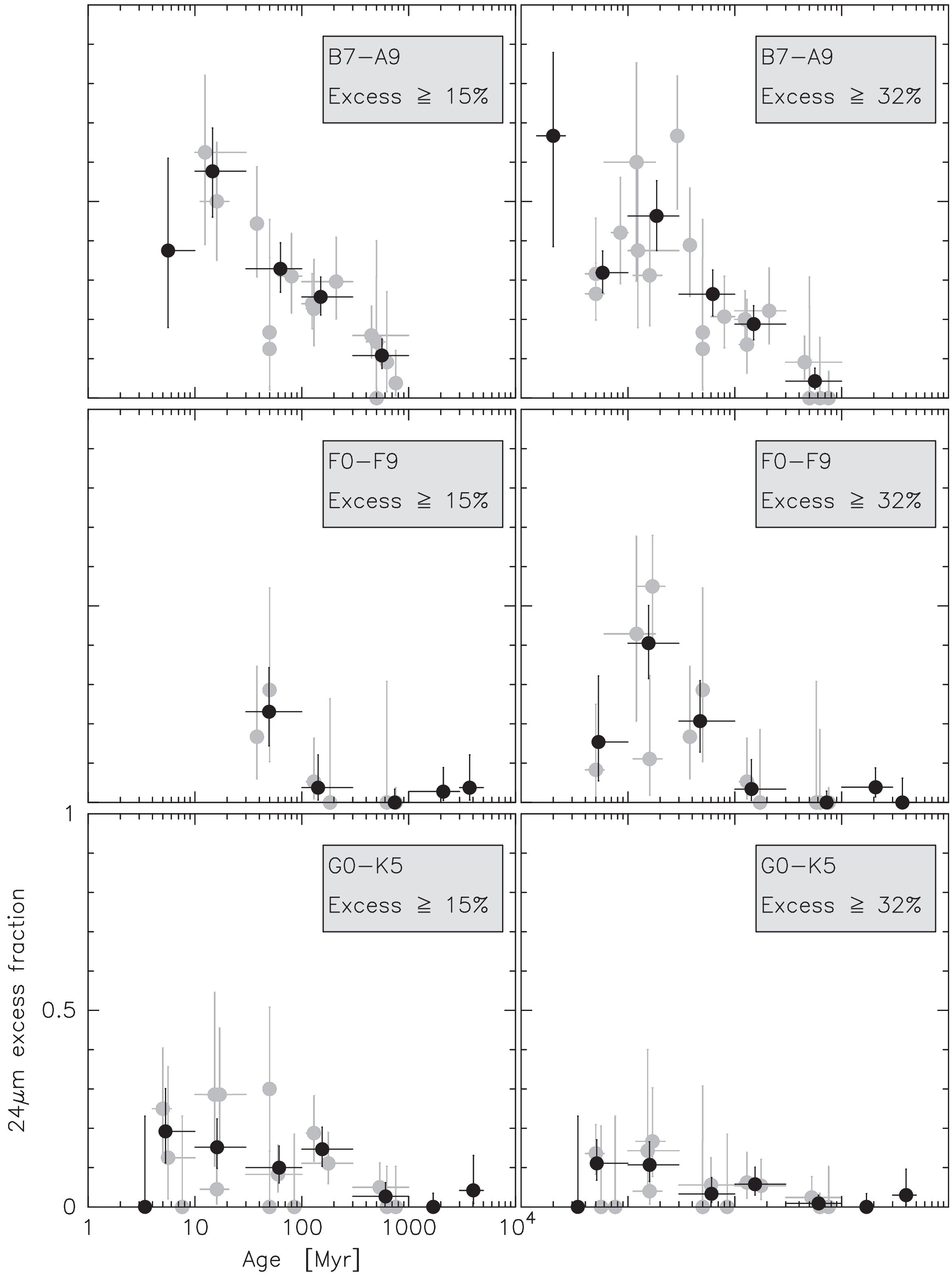

Figure 6. Fraction of sources with a 24 μm excess from a debris disk vs. stellar age for the regions summarized in Table 4. The plots in the left panels show the results for a 24 μm excess detection threshold of 15%, and the right panels for 32%. Results are presented for three spectral type ranges. Gray circles represent individual clusters or associations that contain at least five stars in the appropriate spectral type range. Black circles represent the ensemble average of field stars, clusters, and associations regardless of the sample size.

can be attributed to semantics, as these studies have defined "solar-type" stars as FGK-stars. Whether or not F-stars should be included in the definition of solar-type stars is arbitrary. We treat them separately since there is evidence that the excess fraction of F-type stars is higher than G0-K5 stars. In the 10–30 Myr bin, the excess fraction for F-type stars is 15/37 (41%) at the 32% detection threshold, compared to 6/56 (11%) for G0-K5 star in the same age bin. The probability that these two observed excess fractions are drawn from the same parent population is $p = 0.002$ according to the two-tailed Fisher's exact test.

For B7-A9 and F0-F9 spectral types, the 24 μm excess fraction peaks at $\sim$50% for ages of $\sim$10–30 Myr and a 32% detection threshold. The possible peak in the excess fraction result was noted by Currie et al. (2008b), and the decline in the excess fraction toward older ages was found by Rieke et al. (2005). No such increase is apparent for the G/K stars. Gaspar et al. (2009) found that the excess fraction for F-type stars was greater for ages than 3–10 Myr than for 10–30 Myr, which can be attributed to the high excess fraction for F-type stars in Orion OB1b and Orion OB1a (Hernández et al. 2006). Since Hernández et al. (2006) estimate that the Orion 24 μm observations are complete for stars earlier than F0 in Orion OB1a and A8 in Orion OB1b, the excess fraction for F-stars in Orion may be biased toward higher values and are not included in this analysis.

To evaluate if the excess fraction in the $<$10 Myr and 10–30 Myr age bins could have been drawn from the same parent population for earlier spectral types, we compared the ratios using the two-tailed Fisher's exact test. For a 24 μm excess threshold of 32%, which has the largest sample of stars, the probability that these two age bins are drawn from the parent population is 17% for both B7-A9 and F0-F9 spectral types. If we group B7-F9 spectral types together, the corresponding probability is 9%. The significance of the enhancement in the excess fraction for 10–30 Myr stars relative to $<$10 Myr stars then is $\sim 1.7\sigma$ for stars earlier than F9. Therefore, we conclude that no strong evidence exists for a change in the excess fraction from 2–10 Myr to 10–30 Myr among early-type stars.

6.2. 24 μm Excess

Evolution in the debris disk properties may manifest itself in the excess luminosity as well as the excess fraction. Figure 7 shows the ratio of the 24 μm excess to the photospheric flux as a function of stellar age. Only stars brighter than the photospheric detection limit for the respective samples are shown (see the Appendix). Different symbols are shown for primordial (asterisks) and debris (solid circles) disks; 3σ upper limits are shown for stars without a detected excess (open triangles).

For B/A spectral types, the upper envelope of 24 μm excess emission declines with time. Rieke et al. (2005) suggested that for ages older than 5 Myr, the upper envelope varies with stellar age as t^{-1}, which is shown as the dashed line in the top panel of Figure 7 and extrapolated to younger ages. The relative 24 μm excesses observed around B/A stars in Upper Sco are consistent qualitatively with this upper envelope. For G0-K5 spectral types, the peak relative 24 μm excess is roughly constant for ages less than 300 Myr, with a possible decline toward older ages. For F-type stars, a sharp peak in the 24 μm excess is present at an age of $\sim$16 Myr as previously noted by Hernández et al. (2006) and Currie et al. (2008a). This peak is due to luminous debris disks in the Lower Centaurus Crux association (Chen et al. 2005).

To evaluate the trends quantitatively, we used the generalized Kendall's Tau test as implemented in the ASURV Rev 1.2 package (Lavalley et al. 1992). This test incorporates both the detections and upper limits to make efficient use of the data. We first consider if evolution is present over all ages in the sample. The probability that a correlation of the 24 μm excess versus age is not present for B7-A9, F0-F9, and G0-K5 stars is 3×10^{-10}, 2×10^{-8}, and 10^{-5}, respectively. These results confirm the trend apparent from visual inspection of Figure 7 that the magnitude of the 24 μm excess decreases with stellar age over all spectral types considered here. This conclusion has been reached previously based on *ISO* (Habing et al. 2001; Spangler et al. 2001), *IRAS* (Moór et al. 2006), and *Spitzer* (Rieke et al. 2005; Su et al. 2006; Siegler et al. 2007; Meyer et al. 2008; Carpenter et al. 2009) observations.

We now consider if evolution in the 24 μm excess is present at young ages. We specifically consider the age range between 5 and 17 Myr, which is well populated with clusters and associations, and significant evolution is anticipated based on theoretical models for the collisional evolution of a Kuiper Belt analog (Kenyon & Bromley 2008). For B7-A9, F0-F9, and G0-K5 spectral types, the probability that a correlation of the 24 μm excess versus age is not present between 5 and 17 Myr is 0.14, 0.01, and 0.56, respectively. Thus when subdivided by spectral type, the only suggestion of a trend in the 24 μm excess with age between 5 and 17 Myr is for F-type stars. From inspection of Figure 7, the trend is such that the amount of 24 μm excess increases over this age range.

Currie et al. (2008a) reported a significant rise in the magnitude of the debris emission between 5 and 17 Myr based on debris disk observations around B/A/F stars in Orion OB1b, Orion OB1a, LCC, and UCL. They used the Wilcoxon rank-sum test to determine the probability (p) that the mean excess is consistent between two samples. The strongest statistical trend identified by Currie et al. (2008a) was the increase in the mean 24 μm excess around A/F stars in the 5 Myr Orion OB1b association compared to the 8.5 Myr Orion OB1a association ($p = 0.002$), and Orion OB1b compared to a combined 16–17 Myr old LCC/UCL sample ($p = 0.05$). One difference in the analysis conducted by Currie et al. (2008a) and this study is that we separated the F-type stars from the B/A stars, and we did not include the F-type stars in Orion OB1a and Orion OB1b. While the separation by spectral type is arbitrary from a physical point of view, the observations are complete for B/A spectral types over a broader range of ages. The MIPS 24 μm observations of Orion OB1a and Orion OB1b in particular are complete to the photosphere for F0 and A8 stars (Hernández et al. 2006), respectively, and the 24 μm detections of F-type stars in these associations may be biased toward stars with disks.

We stress that we have not included in this analysis the 17 debris disks identified in the MIPS 24 μm survey of the 13 Myr old, double cluster h & χ Persei (Currie et al. 2008a). These 17 stars have A/F spectral types with relative 24 μm excesses that range between 8 and 180, with a median value of 19. These excesses are extreme compared to the sources shown in Figure 7. These luminous debris disks could conceivably indicate a peak in the debris production in the 10–20 Myr age range. However, the parent sample for the h & χ Persei is about 30 times larger than the Upper Sco sample. As noted by Currie et al. (2008a), the extreme excesses in h & χ Persei may simply reflect better sampling of the same parent luminosity function. Deeper observations and tabulation of the measured flux densities for all cluster members will determine if the extreme excess sources in h & χ Persei represent a peak in the debris production.

6.3. Interpretation

Before drawing further conclusions from the results presented in Section 6.2, we consider how the stellar properties may influence the interpretation of debris disk evolution. The data presented in Figures 6 and 7 were grouped by the observed spectral type. For main-sequence stars, the spectral-type bins of B7-A9, F0-F9, and G0-K5 correspond approximately to stellar masses of 1.9, 1.4, and 0.8 $M_\odot$. The corresponding Kelvin–Helmholtz contraction times are $\sim$ 3, 10, and 30 Myr. Since the

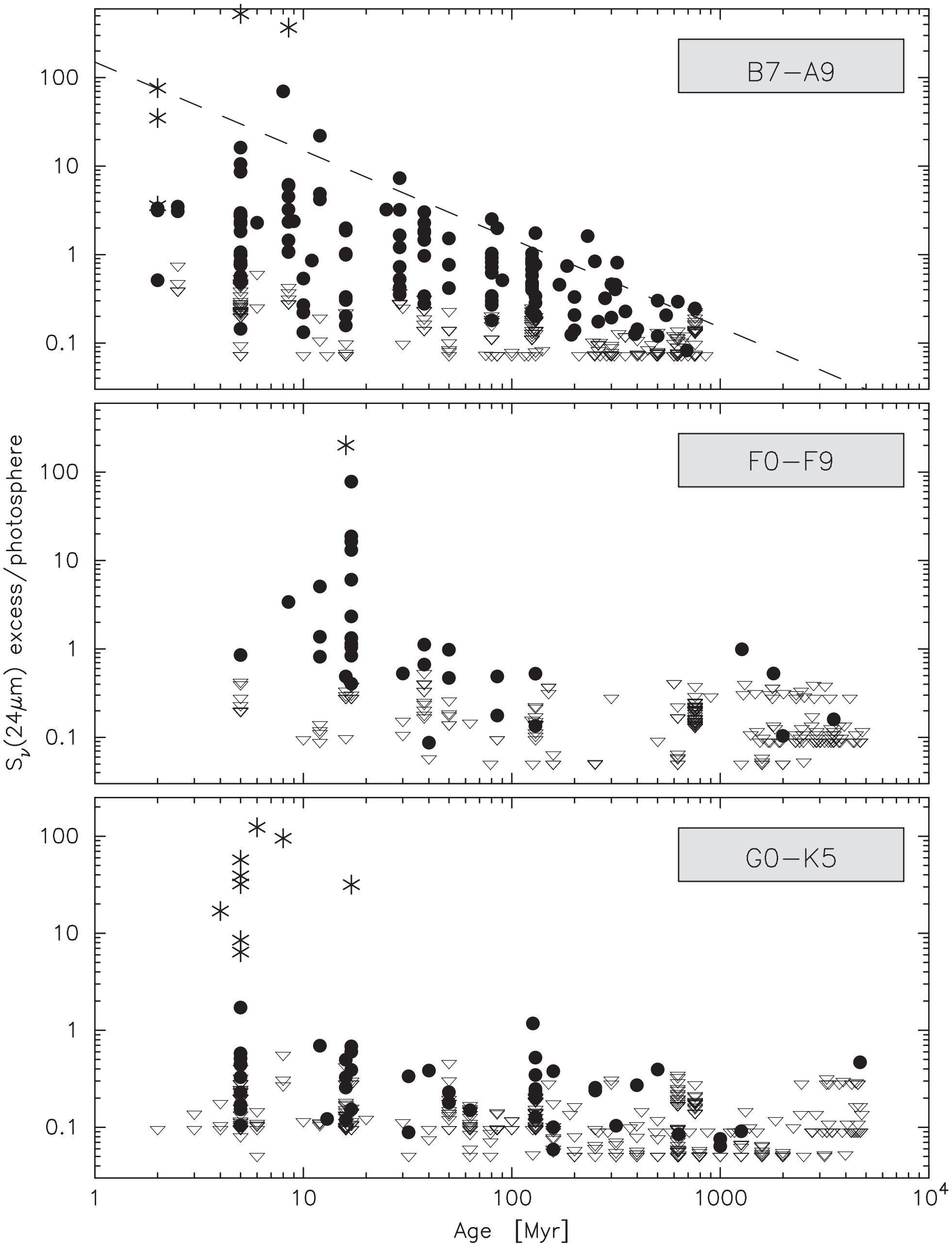

Figure 7. Ratio of the 24 μm excess normalized by the photospheric 24 μm flux density vs. stellar age compiled from the regions summarized in Table 4. Filled circles represent stars with a detected 24 μm excess that are likely debris disks, and open triangles represent 3σ upper limits for stars without excesses. Asterisks indicate optically thick disks (including "anemic" and "evolved" disks). Known Be stars and sources with contaminated 24 μm photometry have been omitted. The dashed line shows the upper envelope to the 24 μm excess from Rieke et al. (2005) for ages older than 5 Myr, and extrapolated here to younger ages.

ages of the stellar samples are as young as 2 Myr, the younger stars are in the pre-main-sequence phase of evolution and the stellar mass and luminosity will vary with age for each of the spectral type bins. This is particularly true for young (<10 Myr) stars more massive than ∼1 $M_\odot$, which are evolving toward the main-sequence along the Henyey tracks. For example, the spectral type for a 2 $M_\odot$ star will be K2, G8, and A2 at an age of 2, 5, and 10 Myr, respectively according to the Siess et al. (2000) pre-main-sequence evolutionary models and Kenyon & Hartmann (1995) temperature scale.

Since the blowout size is proportional to L_*/M_* (see Equation (2)), the minimum grain size in the debris disk will also vary with age. For a fixed spectral type the L_*/M_* ratio, and hence the blowout particle size, decreases by a factor of ∼5 between 1 Myr and 10 Myr for A0-M0 stars. The total grain surface area is proportional to $a_{\rm min}^{-0.5}$ for a $a^{-3.5}$ particle size distribution, and the debris luminosity will thus increase in time if the planetesimal belt is in otherwise steady state.

The expected trends were evaluated more quantitatively using the debris disk model described in Section 5. For a given age and spectral type (i.e., stellar temperature), the stellar mass and luminosity were determined from the Siess et al. (2000) evolutionary models for solar metallicity and no convective overshoot. The 24 μm debris emission was then computed for a planetesimal belt at an orbital radius of 15 AU, with a minimum grain size corresponding to the blowout size. The results are insensitive to the assumed orbital radius since the variations in the debris luminosity with time are caused primarily by changes

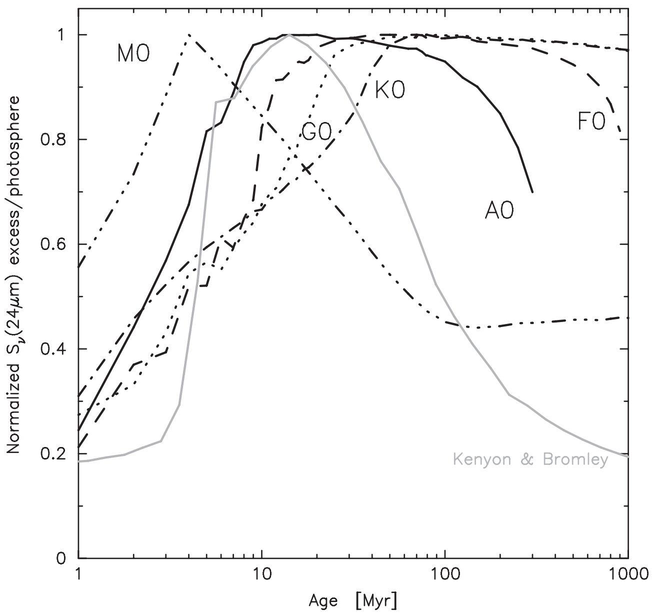

Figure 8. Expected temporal variation in the 24 μm excess relative to the stellar photosphere for A0 (solid black curve), F0 (dashed), G0 (dotted), K0 (dash-dot), and M0 stars (dash-dot-dot-dot) stars. The 24 μm excess for a given curve has been normalized by the peak excess. The stellar mass and luminosity will vary with age for a fixed spectral type as the star evolves toward the main sequence. The stellar parameters for a given age and spectral type were estimated from the Siess et al. (2000) pre-main-sequence models. The model planetesimal belt is at an orbital radius of 15 AU. The debris emission varies in time as stars evolve, which changes the stellar heating and the radiation blowout size. These results show that if the mass of the planetesimal belt is fixed, A-K stars younger than 10 Myr will have a lower 24 μm excess since the smaller grains have been blown out of the system by the greater stellar luminosity. For comparison, the solid gray curve shows the variation in the normalized 24 μm excess from a planetesimal belt with a mass of the minimum mass solar nebula that extends between 30 and 150 AU around a 2 $M_\odot$ star with constant stellar luminosity (Kenyon & Bromley 2008).

in the grain surface area. We assume that the minimum grain size in the debris disk varies instantaneously as stars evolve since the collisional lifetime of dust within an orbital radius of 30 AU is less than 1 Myr for observed debris disks (Backman & Paresce 1993). In this manner, the variation in the 24 μm excess relative to the photosphere was computed considering only stellar evolution.

Figure 8 shows the results of the model calculations. For A0 through K0 stars, the relative 24 μm excess increases by a factor of ∼5 from an age of 1 Myr to a peak at 10–50 Myr. The peak relative excess is reached sooner around earlier spectral types since the stars reach the main sequence on shorter timescales. M-type stars obtain a peak relative excess in only a few million years when the grain blowout size is less than 0.05μm. At this point, any grains removed by radiation pressure are inefficient emitters at 24 μm, and the debris luminosity declines with the stellar luminosity.[7] If the model assumptions are correct, the sensitivity functions presented in Figure 8 will be superimposed on the evolution of the debris luminosity and must be considered when attributing any increase in the debris luminosity with age to planet formation.

For comparison, the gray solid line in Figure 8 shows the variation in the 24 μm excess relative to the photosphere for a 2 $M_\odot$ star (∼A3 spectral type) with a planetesimal belt between 30 and 150 AU from the Kenyon & Bromley (2008) models. Since the stellar luminosity is held constant in these models, the temporal variation in the infrared luminosity results from changes in the debris production. The debris evolution in these models depends on the stellar mass and the planetesimal belt properties (mass, orbital radius), but the general prediction is that the fractional debris luminosity rises at early ages, and declines at later times. The results show that for a 30–150 AU planetesimal belt, the rise in the debris luminosity and the age where debris production is maximized resembles the evolutionary curve expected based on stellar evolution alone. Clear differences are observed at older ages where the debris luminosity in the Kenyon & Bromley (2008) models declines more rapidly.

We now evaluate if the magnitude of the relative 24 μm excess varies with stellar age for ages $<$ 20 Myr, and if any increase can be attributed to stellar evolution. For both the B7-A9 and G0-K5 spectral-type ranges, any variations in the 24 μm excess with age between ages of 5 and 17 Myr have a significance of less than 2σ (see Section 6.2 and Figure 7). Thus independent of the selection function presented in Figure 8, no compelling evidence exists for a variation in the mean relative 24 μm excess for B7-A9 and G0-K5 stars in that age range.

The F-type stars show the strongest evidence (2.6σ) for a rise in the relative 24 μm excess (see Section 6.2), but these results need to be interpreted in view of the expected increase in the debris emission shown in Figure 8. For the F-type stars between ages of 5 and 17 Myr, we scaled the magnitude of the 24 μm excess by the inverse of the model calculations computed for a F5 star, which corrects for the reduced excess emission expected to occur with stellar evolution. The probability of a trend in the observed excess emission with age (see Figure 7) was then recomputed using the Kendall Tau test. We find the probability that a correlation is not present increases from $p = 0.01$ (2.6σ) to $p = 0.02$ (2.3σ).

In summary, we conclude that any evidence for an increase in the 24 μm debris emission with age between 5 and 17 Myr rests primarily with F-type stars, and the significance is $\lesssim 2.6\sigma$. Any variations in the relative 24 μm excess over this age range for B/A and G/K are significant at less than 2σ confidence. Given the low statistical significance and that the increasing relative excess is observed in a narrow spectral-type range, we hesitate to ascribe the apparent rise in the mean relative 24 μm excess among F-stars to the onset of planetesimal stirring.

6.4. Debris Disks Around M-Stars

Evolution of debris emission around M-stars is more difficult to quantify since most MIPS surveys are insensitive to the stellar photosphere for these spectral types. Nonetheless, for completeness, we present in Figure 9 the 24 μm excess relative to photosphere as a function of age for M0–M5 stars in IC 348 (Lada et al. 2006), σ Ori (Hernández et al. 2007), Upper Sco, η Cha (Gautier et al. 2008), TW Hydra moving group (Low et al. 2005), NGC 2547 (Forbrich et al. 2008), and IC 2391 (Siegler et al. 2007). M-stars with upper limits to the 24 μm excess are not shown for clarity, and because most studies have not reported upper limits if a star is not detected.

Figure 9 again illustrates the dichotomy at young ages between classified primordial disks (asterisks) and debris disks (filled circles). The 24 μm excess around Upper Sco M-stars is comparable to many of the stars in NGC 2547 at an age of ∼ 38 Myr (Naylor & Jeffries 2006). However, five M-stars in

[7] MIPS observations have yielded a small number of debris disks around young, low-mass T Tauri stars (Cieza et al. 2007). The low excess needs to be interpreted in context of these model calculations, which predict the 24 μm excess will be 5 times weaker than a 10 Myr star if the planetesimal belt is otherwise the same.

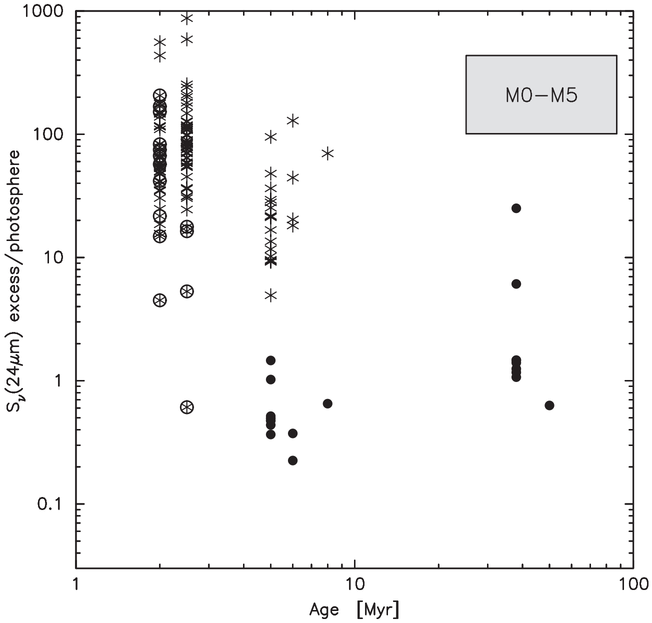

Figure 9. 24 μm excess for M0–M5 stars as a function of stellar age. Excess sources are shown for IC 348 (age 2 Myr; Lada et al. 2006), σ Ori (2.5 Myr; Hernández et al. 2007), Upper Sco (5 Myr), η Cha (6 Myr; Gautier et al. 2008), TW Hydra moving group (8 Myr; Low et al. 2005), NGC 2547 (38 Myr; Forbrich et al. 2008), and IC 2391 (50 Myr; Siegler et al. 2007). Asterisks indicate stars where the 24 μm excess is thought to originate from an optically thick disk; circled asterisks are optically thick disks further subdivided as "anemic" or "evolved" disks. Filled circles indicate stars classified as debris systems. M-stars with upper limits at 24 μm have been omitted for clarity. Not all surveys shown here are sensitive to the stellar photosphere, and this diagram should not be used to infer the evolution of debris emission around M-type stars.

NGC 2547 have a 24 μm excess of ∼10 times the photosphere; three of these five stars have been observed with IRAC (Young et al. 2004), and one has an 8 μm excess. By contrast, all of the Upper Sco sources classified with a primordial disk have an 8 μm excess. It would be unusual for an optically thick disk to persist for ∼ 38 Myr, and the debris disk is a reasonable interpretation for the NGC 2547 sources. These results suggest that distinguishing primordial disks from debris disks for M-type stars merits a more detailed examination (cf. Ercolano et al. 2009).

7. SUMMARY

We have presented the results of a *Spitzer* 24 μm and 70 μm photometric survey of 205 members of the Upper Scorpius OB association. These data were combined with MIPS photometry for 15 Upper Sco sources observed by the FEPS Legacy program to provide a census of circumstellar disks around stars with spectral ranges ranking from B0 to M5 at an association age of 5 Myr (Preibisch et al. 2002). By analyzing the 24 μm photometry with 4.5 μm and 8 μm measurements presented in Paper I, we identify 54 stars that have observed 24 μm emission that exceeds the expected stellar photospheric emission by 32% or more. Similarly, 12 stars were identified with a $\geqslant 3\sigma$ photometric excess at 70 μm; all 12 of these stars have a detectable 24 μm excess.

The nature of the excess sources was established based on the color and magnitude of the excess emission. We find a dichotomy of excess characteristics. One population, found only around the K- and M-type stars, has strong excess emission at both 8 μm and 24 μm that is comparable to known optically thick circumstellar disks. A second population, found around all spectral types, has weak 8 μm and 24 μm excesses compared to optically thick and "anemic" disks in the IC 348 cluster (Lada et al. 2006). We suggest that these weak excesses originate from debris disks formed from the collisional shattering of planetesimals, although we cannot exclude the possibility that these systems are the remnants of optically thick disks. Of the 54 excess stars, we attribute the 24 μm excess emission to two Be stars, 24 primordial disks, and 28 debris disks. The debris disks include 11 K/M stars.

The debris disks were analyzed to investigate whether the orbital radius of the presumed planetesimal belts vary systematically with spectral type. We modeled the emission with a power-law distribution of grain sizes following the Dohnanyi (1969) equilibrium distribution ($n(a) \propto a^{-3.5}$). The orbital radius (R) and grain size distribution (N_o; see Equation (1)) were set to reproduce the observed excess emission around nine B/A stars with infrared excesses at both 16 μm and 24 μm. The expected emission around stars of other spectral types were then estimated after allowing for variations in the stellar heating and radiation blowout of small grains. We find that the magnitude of the 24 μm emission observed around later stars can be produced by this model, indicating it is not necessary to invoke a different radial distribution. This model predicts a steep fall off in the relative 24 μm excess for stars earlier than ∼ B7 due to blowout of the small grains, and later than ∼ M0 due to reduced stellar heating.

The Upper Sco results are combined with other *Spitzer* 24 μm surveys in the literature to reassess the evolution of 24 μm debris emission. After consideration of both sample sizes and detection limits, we find a decline in the magnitude of the 24 μm excess relative to the photosphere for spectral types between B7 and K5 and ages between 10 Myr and 5 Gyr, as has been noted in previous studies (Habing et al. 2001; Decin et al. 2003; Rieke et al. 2005; Carpenter et al. 2009). We also investigated if the 24 μm excess increases with stellar age for ages $\lesssim$ 20 Myr. Such an increase may be indicative of the onset of planetesimal stirring (Kenyon & Bromley 2008). We caution, however, that a similar increase in the excess emission may also result from pre-main-sequence evolution; for a fixed spectral type, the L_*/M_* ratio will decrease with age, which leads to a higher debris luminosity as fewer grains are ejected by radiative forces. The observed mean 24 μm excess around F-type stars increases between ages of 5 and 17 Myr as previously found by Currie et al. (2008a, see also Hernández et al. 2006), but with a significance of ∼ 2.3σ–2.6σ confidence. The variations in the mean 24 μm excess around B/A and G/K stars over the same age range are significant at less than 2σ confidence. We conclude that the observational data do not yet require a physical mechanism to produce a peak in the observed debris emission.

We are grateful to Scott Kenyon for his comments on the manuscript. This work is based on observations made with the *Spitzer Space Telescope*, which is operated by JPL/Caltech under a contract with NASA. Support for this work was provided by NASA through an award issued by JPL/Caltech. This research made use of the SIMBAD database, the IRSA archive, and the Two Micron All Sky Survey.

APPENDIX

COMPILATION OF *SPITZER* DEBRIS DISK SURVEYS

To compare the Upper Sco results with previous observations, we compiled data from published *Spitzer* 24 μm surveys

Table 4
Compilation of Debris Disk Surveys

Region	Age (Myr)	Age Reference	Nstars	Minimum Excess[a] (%)	SpT Early[b]	SpT Limit[c]	Photometry Reference
CrA	2-16	21	7	10	G6	K5	4
IC 348	2	17	6	30	A0	A4	15
σ Ori	2.5	29	11	39	B2	A3	13
Upper Sco	5 ± 1	25	220	32	B0	M5	34
			5	30	F0	G5	5
			16	10	G0	K3	4
			3	8	B9	B8	32
Orion OB1b	5 ± 1	3	21	31	B1	A8	12
η Cha	6 ± 2	18	16	31	B8	M5.75	9
			1	8	B8	B8	5
TW Hya	8	37	24	60	A0	M5	16
Orion OB1a	8.5 ± 1.5	3	21	32	B1	F0	12
β Pic	12 ± 6	36	30	27	A0	M4.5	27
			3	10	F8	K7	4
			2	10	A0	A5	32
UCL	16	26	11	30	F0	G8	5
			23	10	F8	K3	4
			16	8	B7	A2	32
LCC	17	26	24	30	F0	G5	5
			14	10	G0	K2	4
NGC 2232	29 ± 4	19	15	30	B1	A8	7
Tucana-Horologium	30	20	9	27	B8	M3	27
NGC 2547	38 ± 5	22	31	15	B9	F5	11
IC 2391	50 ± 5	1	29	15	B3	K4	30
IC 2602[d]	50 ± 5	1,31	7	8	B6	B9	32
			5	10	G0	K0	4
NGC 2422	80 ± 20	35	31	15	B5	A	28
α Per	85 ± 10	1	13	10	F5	K2	4
			5	8	B8	A0	32
Pleiades	130 ± 20	1	20	10	F6	K2	4
			72	15	B6	K3	10
			6	8	B8	A0	32
NGC 2516	125 ± 25	19	51	15	B8.5	F0	28
Ursa Major	500 ± 100	14	7	8	A0	A6	32
Coma Berenices	500 ± 100	23	5	8	A2	A4	32
Hyades	625 ± 50	24	78	18	A1	K7	6
			22	10	F8	K2	4
			11	8	A1	A7	32
Praesepe	757 ± 36	8	90	15	A1	G6	8
			5	8	A0	A6	32
Field	150–4570	2	38	30	F0	K5	2
	3–4000	21	186	10	F5	K7	4
	5–680	28	30	15	B7	A5	28
	5–850	32	85	8	B7	A7	32
	190–5000	33	98	10	F0	K4.5	33

Notes.
[a] The minimum percent 24 μm flux density above the photosphere used to identify an excess.
[b] Earliest spectral type in the survey.
[c] Latest spectral type where the minimum excess could be detected.
[d] We adopt an age of 50 Myr for IC 2391, and assume IC 2391 and IC 2602 have the same age following Stauffer et al. (1997).
References. (1) Barrado y Navascués et al. 2004; (2) Beichman et al. 2006; (3) Briceño et al. 2005; (4) Carpenter et al. 2008; (5) Chen et al. 2005; (6) Cieza et al. 2008; (7) Currie et al. 2008b; (8) Gaspar et al. 2009; (9) Gautier et al. 2008; (10) Gorlova et al. 2006; (11) Gorlova et al. 2007; (12) Hernández et al. 2006; (13) Hernández et al. 2007; (14) King et al. 2003; (15) Lada et al. 2006; (16) Low et al. 2005; (17) Luhman et al. 2003; (18) Luhman & Steeghs 2004; (19) Lyra et al. 2006; (20) Mamajek et al. 2004; (21) Meyer et al. 2006; (22) Naylor & Jeffries 2006; (23) Odenkirchen et al. 1998; (24) Perryman et al. 1998; (25) Preibisch et al. 2002; (26) Preibisch & Mamajek 2008; (27) Rebull et al. 2008; (28) Rieke et al. 2005; (29) Sherry et al. 2008; (30) Siegler et al. 2007; (31) Stauffer et al. 1997; (32) Su et al. 2006; (33) Trilling et al. 2008; (34) This study; (35) van Rensbergen et al. 1978; (36) Zuckerman et al. 2001; (37) Zuckerman & Song 2004.

for debris disks. We considered studies in which the parent sample is not biased for or against the presence of a debris disk. This requirement implies that the parent sample must have been selected by photospheric indicators, and that the *Spitzer* observations were sensitive to the stellar photosphere. In practice, this is not strictly true for nearby moving group such as β Pic, η Cha, and TW Hydra, where the moving group was initially identified based on the presence of an apparently isolated sources with an prominent infrared excess. We nonetheless include these groups since the subsequent surveys for moving group members were not biased toward circumstellar disks.

Table 4 summarizes the surveys that were compiled and contain five stars or more. We include in this table the name of the region, the adopted age, the earliest spectral type in the survey, the latest spectral type at which the photosphere can be reliable detected as discussed above, the number of stars in this spectral-type range, and the minimum 24 μm excess above the stellar photosphere that could be detected. In some regions (e.g., NGC 2232, Pleiades, Praesepe), not all stars have spectral types available from spectroscopic observations, and the spectral type was estimated from optical or near-infrared colors. Field stars with ages between 3 Myr and 5 Gyr were compiled from the FEPS survey of solar-type stars (Meyer et al. 2006), the survey of solar-type field stars by Beichman et al. (2006) and Trilling et al. (2008), and the survey of B/A stars by Rieke et al. (2005) and Su et al. (2006).

The photometry was extracted from the publications listed in Table 4. No attempt was made to re-reduce the data under a common data reduction method or to re-assess cluster or association membership. Several studies noted sources where the photometry was contaminated by nebulosity or a companion sources. If these stars were excluded from the analysis in the original study, they were also excluded in our analysis. After compiling the source lists, we ran all source names through SIMBAD to identify duplicate sources appearing under different names. If photometry appear for a star in more than one survey, we adopted the photometry from the survey with the higher signal to noise.

Most *Spitzer* studies have identified sources with excesses based on the presence of unusually red infrared colors (e.g., [K]–[24], [8]–[24]). Each study has a minimum detectable excess that depends on the depth of the survey, the presence of nebulosity in sky background, the distance to the stellar sample, and the intrinsic brightness of the star. In nearly all cases, we adopted the limiting thresholds adopted in the original study to identify 24 μm excesses, which is normally taken to be three or four times the rms scatter around the main locus of data points in a color–color diagram or a stellar color that is thought to represent photospheric colors (see, e.g., Figure 1). We then identified the latest spectral type in which the internal uncertainty in the measured photospheric flux was less than this rms scatter. This criteria removed sources where the photometric uncertainty was comparable to the excess being measured. If the threshold to identify an excess ($\equiv \Delta$) was expressed in magnitudes, the adopted threshold was estimated as $10^{\Delta/2.5}$.

The ages for clusters and associations were adopted from the literature based on a number of techniques, including pre-main-sequence evolutionary tracks, lithium depletion, and the main sequence turnoff point. The age uncertainties were adopted from the literature, but if no uncertainty was quoted, we assumed an age uncertainty of 0.3 dex in the logarithm of the age. The age uncertainties for the clusters and associations do not reflect any systematic uncertainty associated with the particular method. The ages for field stars were adopted from the studies presenting the *Spitzer* data. The references for the ages are provided in Table 4.

A few studies are not included in this comparison since the observations could not be analyzed in a consistent manner. First, we did not include surveys where the observations were not sensitive to the photosphere for spectral types A or later, either because the regions are more distant than $\sim$ 900 pc (Trumpler 37 and NGC 7160, Sicilia-Aguilar et al. 2006; h & χ Persei, Currie et al. 2008a; NGC 2262, Currie et al. 2008b), or the observations were exclusively of late spectral types (λ Orionis; Barrado y Navascués et al. 2007). MIPS 24 μm observations of the γ Velorum cluster were not incorporated; while the observations were sensitive to the photosphere for stars early than $\sim$F8, the contamination from field stars is non-negligible (Hernández et al. 2008). We also did not analyze MIPS observations of weak-lined T Tauri stars since the samples excluded optically thick disks (Padgett et al. 2006; Cieza et al. 2007).

Given the heterogeneous nature of the analyzes to identify *Spitzer* excesses, we occasionally had to re-analyze data from the original study to provide a uniform analysis. The following discussion summarizes the regions where we re-interpreted the observations.

σ Orionis. From the photometry presented by Hernández et al. (2007), 97% (33 out of 34) stars brighter than $J = 10.2$ mag were detected at 24 μm, while only four of seven stars between $J =$ 10.2 and 10.5 mag were detected. The completeness limit was then defined as $J = 10.2$. For stars fainter than $J = 10.2$, the bluest star has a dereddened color of $J - H = 0.15$. Therefore, we assumed the survey is complete for $J - H <= 0.15$, corresponding to spectral type earlier than F0.

IC 348. Of the eight A-type stars in IC 348 studied by Lada et al. (2006), six were detected by at 24μm, one was not observed at 24 μm, and one has an upper limit from locally bright background. Only 57% of the FG stars and less than 33% of the KM stars in IC 348 have 24 μm measurements, and therefore only the A-stars in IC 348 were included. We adopted a detection threshold of 30% for a 24 μm excess based on Figure 7 in Lada et al. (2006).

NGC 2232. Currie et al. (2008b) estimated a 5σ and 10σ detection limit of 10.5 mag and 9.75 mag for their 24 μm survey. They also find that the number of sources detected at 24 μm falls rapidly for sources fainter than [24] = 10.5. We therefore adopted [24] = 10 mag as a limiting magnitude, and find that 99% of stars brighter than $J = 10$ mag have a MIPS 24 μm detection brighter than this limit. For a distance of 340 pc, an age of 25 Myr, and a color excess of $E(B - V) = 0.07$, $J = 10$ corresponds roughly to a A8 star, which we adopt as the completeness limit of the survey. The rms scatter in the $K-$[24] color for stars brighter than the completeness limit and not containing an infrared excess (as defined in Currie et al. 2008b) is 0.09 mag, which was adopted as the photometric uncertainty.

Praesepe. From Figure 6 in Gaspar et al. (2009), we find that the number of stars with unphysical blue stellar colors increases for stars redder than $r - K_s = 1.5$. We consider only stars bluer than this limit, which corresponds to stars earlier than G5.

REFERENCES

Backman, D. E., & Paresce, F. 1993, in Protostars and Planets III, ed. E. H. Levy & K. L. Lunine (Tucson, AZ: Univ. Arizona Press), 1253
Barrado y Navascués, D., Stauffer, J. R., & Jayawardhana, R. 2004, ApJ, 614, 368
Barrado y Navascués, D., et al. 2007, ApJ, 664, 481
Beichman, C. A., et al. 2006, ApJ, 652, 1674
Briceño, C., Calvet, N., Hernández, J., Vivas, A. K., Hartmann, L., Downes, J. J., & Berlind, P. 2005, AJ, 129, 907
Bryden, G., et al. 2006, ApJ, 636, 1098
Bouy, H., & Martín, E. L. 2009, A&A, 504, 981
Burns, J. A., Lamy, P. L., & Soter, S. 1979, Icarus, 40, 1
Cardelli, J. A., Clayton, G. C., & Mathis, J. S. 1989, ApJ, 345, 245

Carpenter, J. M., Mamajek, E. E., Hillenbrand, L. A., & Meyer, M. R. 2006, ApJ, 651, L49 (Paper I)
Carpenter, J. M., et al. 2008, ApJS, 179, 423
Carpenter, J. M., et al. 2009, ApJS, 181, 197
Chapman, N. L., Mundy, L. G., Lai, S., & Evans, N. J. 2009, ApJ, 690, 496
Chen, C. H., Jura, M., Gordon, K. D., & Blaylock, M. 2005, ApJ, 623, 493
Cieza, L. A., Cochran, W. D., & Augereau, J.-C. 2008, ApJ, 679, 720
Cieza, L. A., et al. 2007, ApJ, 667, 308
Crampton, D. 1968, AJ, 73, 337
Currie, T., & Kenyon, S. J. 2009, AJ, 138, 703
Currie, T., Kenyon, S. J., Balog, Z., Rieke, G., Bragg, A., & Bromley, B. 2008a, ApJ, 672, 558
Currie, T., Lada, C. J., Plavchan, P., Robitaille, T. P., Irwin, J., & Kenyon, S. J. 2009, ApJ, 698, 1
Currie, T., Plavchan, P., & Kenyon, S. J. 2008b, ApJ, 688, 597
Dahm, S., & Carpenter, J. M. 2009, AJ, 137, 4024
Decin, G., Dominik, C., Waters, L. B. F. M., & Waelkens, C. 2003, ApJ, 598, 636
de Zeeuw, P. T., Hoogerwerf, R., de Bruijne, J. H. L., Brown, A. G. A., & Blaauw, A. 1999, AJ, 117, 354
Dohnanyi, J. W. 1969, J. Geophys. Res., 74, 2531
Dominik, C., & Decin, G. 2003, ApJ, 598, 626
Engelbracht, et al. 2007, PASP, 119, 994
Ercolano, B., Clarke, C. J., & Robitaille, T. P. 2009, MNRAS, 394, L141
Espaillat, C., Calvet, N., D'Alessio, P., Hernández, J., Qi, C., Hartmann, L., Furlan, E., & Watson, D. M. 2007, ApJ, 670, L135
Forbrich, J., Lada, C. J., Muench, A. A., & Teixera, P. S. 2008, ApJ, 687, 1107
Gaspar, A., et al. 2009, ApJ, 697, 1578
Gautier, T. N., III, Rebull, L. M., Stapelfeldt, K. R., & Mainzer, A. 2008, ApJ, 683, 813
Gautier, T. N., III, et al. 2007, ApJ, 667, 527
Gorlova, N., Balog, Z., Rieke, G. H., Muzerolle, J., Su, K. Y. L., Ivanov, V. D., & Young, E. T. 2007, ApJ, 670, 516
Gorlova, N., et al. 2006, ApJ, 649, 1028
Gustafson, B. A. S. 1994, Ann. Rev. Earth Planetary Sci., 22, 553
Habing, H. J., et al. 2001, A&A, 365, 545
Hernández, J., Calvet, N., Hartmann, L., Briceño, C., Sicilio-Aguilar, A., & Berlind, P. 2005, AJ, 129, 856
Hernández, J., Hartmann, L., Calvet, N., Jeffries, R. D., Gutermuth, R., Muzerolle, J., & Stauffer, J. 2008, ApJ, 686, 1195
Hernández, J., et al. 2006, ApJ, 652, 472
Hernández, J., et al. 2007, ApJ, 662, 1067
Holland, W. S., et al. 1998, Nature, 392, 788
Houk, N. 1982, Michigan Catalogue of Two-Dimensional Spectral Types for the HD Stars, Vol. 3 (Ann Arbor, MI: Univ. Michigan)
Houk, N., & Smith-Moore, M. 1988, Michigan Catalogue of Two-Dimensional Spectral Types for the HD stars, Vol. 4 (Ann Arbor, MI: Univ. Michigan)
Jaschek, C., Jaschek, M., & Kucewicz, B. 1964, Z. Astrophys., 59, 108
Kenyon, S. J., & Bromley, B. C. 2004, AJ, 127, 513
Kenyon, S. J., & Bromley, B. C. 2008, ApJS, 179, 451
Kenyon, S. J., & Hartmann, L. 1995, ApJ, 101, 117
King, J., Villarreal, A. R., Soderblom, D. R., Gulliver, A. F., & Adelman, S. J. 2003, AJ, 125, 1980
Köhler, Kunkel M., Leinert, C., & Zinnecker, H. 2000, A&A, 356, 541
Kunkel, M. 1999, PhD thesis, Julius-Maximilians-Universität Würzburg
Lada, C. J., et al. 2006, AJ, 131, 1574
Lagrange, A., Backman, D. E., & Artymowicz, P. 2000, in Protostars and Planets IV, ed. V. Mannings, A. Boss, & S. S. Russell (Tucson, AZ: Univ. Arizona Press), 639
Lavalley, M., Isobe, T., & Feigelson, E. 1992, in ASP Conf. Ser. 25, Astronomical Data Analysis Software and Systems I, ed. D. M. Worrall, C. Biemesderfer, & J. Barnes (San Francisco, CA: ASP), 245
Liou, J.-C., & Zook, H. A. 1999, AJ, 118, 580
Löhne, T., Krivov, A. V., & Rodmann, J. 2008, ApJ, 673, 1123
Low, F. J., Smith, S., Werner, M., Chen, C., Krause, V., Jura, M., & Hines, D. C. 2005, ApJ, 631, 1170
Luhman, K. L., Stauffer, J. R., Muench, A. A., Rieke, G. H., Lada, E. A., Bouvier, J., & Lada, C. J. 2003, ApJ, 493, 1093
Luhman, K. L., & Steeghs, D. 2004, ApJ, 609, 917
Lyra, W., Moitinho, A., van der Bliek, N. S., & Alves, J. 2006, A&A, 453, 101
Makovoz, D., & Marleau, F. R. 2005, PASP, 117, 1113
Mamajek, E. E., Meyer, M. R., Hinz, P. M., Hoffmann, W. F., Cohen, M., & Hora, J. L. 2004, ApJ, 612, 496
Martín, E. L. 1998, AJ, 115, 351
Mathis, J. S. 1990, ARA&A, 28, 37
Meyer, M. R., Backman, D. E., Weinberger, A. J., & Wyatt, M. C. 2007, in Protostars and Planets V, ed. B. Reipurth, D. Jewitt, & K. Keil (Tucson, AZ: Univ. Arizona Press), 573
Meyer, M. R., et al. 2006, PASP, 118, 1690
Meyer, M. R., et al. 2008, ApJ, 673, 181
Moór, A., Ábrahám, P., Derekas, A., Kiss, Cs., Kiss, L. L., Apai, D., Grady, C., & Henning, Th. 2006, ApJ, 644, 525
Najita, J., & Williams, J. P. 2005, ApJ, 635, 625
Naylor, T. 1998, MNRAS, 296, 339
Naylor, T., & Jeffries, R. D. 2006, MNRAS, 373, 1251
Odenkirchen, M., Soubiran, C., & Colin, J. 1998, New Astron., 3, 583
Odenwald, S. F. 1986, ApJ, 307, 711
Padgett, D. L., et al. 2006, ApJ, 645, 1283
Papovich, C., et al. 2004, ApJS, 154, 70
Pascucci, I., et al. 2006, ApJ, 651, 1177
Perryman, M. A. C., et al. 1998, A&A, 331, 81
Plavchan, P., Jura, M., & Lipscy, S. J. 2005, ApJ, 631, 1161
Plavchan, P., et al. 2009, ApJ, 698, 1068
Porter, J. M., & Rivinius, T. 2003, PASP, 115, 1153
Preibisch, T., Brown, A. G. A., Bridges, T., Guenther, E., & Zinnecker, H. 2002, AJ, 124, 404
Preibisch, T., Guenther, E., & Zinnecker, H. 2001, AJ, 121, 1040
Preibisch, T., Guenther, E., Zinnecker, H., Sterzik, M., Frink, S., & Roeser, S. 1998, A&A, 333, 619
Preibisch, T., & Mamajek, E. 2008, in Handbook of Star Forming Regions, Vol. II, ed. Bo Reipurth (San Francisco, CA: ASP), 235
Preibisch, T., & Zinnecker, H. 1999, AJ, 117, 2381
Rebull, L. M., et al. 2008, ApJ, 681, 1484
Rhee, J., Song, I., Zuckerman, B., & McElwain, M. 2007, ApJ, 660, 1556
Rieke, G. H., et al. 2005, ApJ, 620, 1010
Scholz, A., Jayawardhana, R., Wood, K., Meeus, G., Stelzer, B., Walker, C., & O'Sulliivan, M. 2007, ApJ, 660, 1517
Sherry, W. H., Walter, F. M., Wolk, S. J., & Adams, N. R. 2008, AJ, 135, 1616
Sicilia-Aguilar, A., et al. 2006, ApJ, 638, 897
Siegler, N., et al. 2007, ApJ, 654, 580
Siess, L., Dufour, E., & Forestini, M. 2000, A&A, 358, 593
Skrutskie, M. F., et al. 2006, AJ, 131, 1163
Spangler, C., Sargent, A. I., Silverstone, M. D., Becklin, E. E., & Zuckerman, B. 2001, ApJ, 555, 932
Stauffer, J. R., et al. 1997, ApJ, 479, 776
Strom, K. M., Strom, S. E., Edwards, S., Cabrit, S., & Skrutskie, M. F. 1989, AJ, 97, 1451
Strubbe, L. E., & Chiang, E. I. 2006, ApJ, 648, 652
Su, K. Y. L., et al. 2006, ApJ, 653, 675
Takeuchi, T., & Artymowicz, P. 2001, ApJ, 557, 990
Trilling, D. E., et al. 2008, ApJ, 674, 1086
van der Bliek, N. S., Manfroid, J., & Bouchet, P. 1996, A&AS, 119, 547
van Rensbergen, W., Hammerschlag-Hensberge, G., & van den Heuvel, E. P. J. 1977, A&A, 64, 131
Walter, F. M., Vrba, F. J., Mathieu, R. D., Brown, A., & Myers, P. C. 1994, AJ, 107, 692
Weingartner, J. C., & Draine, B. T. 2001, ApJ, 548, 296
Werner, M., Fazio, G., Rieke, G., Roellig, T. L., & Watson, D. M. 2006, ARA&A, 44, 269
Werner, M., et al. 2004, ApJS, 154, 1
Williams, D. R., & Wetherill, G. W. 1994, Icarus, 107, 117
Wood, B. E. 2004, Living Rev. Solar Phys., 1, 2
Wyatt, M. C. 2003, ApJ, 598, 1321
Wyatt, M. C. 2008, ARA&A, 46, 339
Wyatt, M. C., Smith, R., Greaves, J. S., Beichman, C. A., Bryden, G., & Lisse, C. M. 2007a, ApJ, 658, 569
Wyatt, M. C., Smith, R., Su, K. Y. L., Rieke, G. H., Greaves, J. S., Beichman, C. A., & Bryden, G. 2007b, ApJ, 663, 365
Young, E. T., et al. 2004, ApJS, 154, 428
Zuckerman, B., Forveille, T., & Kastner, J. H. 1995, Nature, 373, 494
Zuckerman, B., & Song, I. 2004, ARA&A, 42, 685
Zuckerman, B., Song, I., Bessell, M. S., & Webb, R. A. 2001, ApJ, 562, L87